Vorticity dynamics of dilute two-way-coupled particle-laden mixing layers

By E. MEIBURG[1,2]†, E. WALLNER[1,3], A. PAGELLA[1,4],
A. RIAZ[1], C. HÄRTEL[2] AND F. NECKER[2]

[1]Department of Aerospace and Mechanical Engineering, University of Southern California,
Los Angeles, CA 90089-1191, USA

[2]Institute of Fluid Dynamics, Swiss Federal Institute of Technology, ETH Zentrum,
CH-8092 Zürich, Switzerland

[3]Present address: Institute of Flight Mechanics and Flight Control, University of Stuttgart,
Pfaffenwaldring 7a, D-70550 Stuttgart, Germany

[4]Present address: Institute of Aero- and Gasdynamics, University of Stuttgart,
Pfaffenwaldring 21, D-70550 Stuttgart, Germany

The two-way coupling mechanisms in particle-laden mixing layers are investigated, with and without particle settling, and with an emphasis on the resulting modifications to the fluid vorticity field. The governing equations are interpreted with respect to the production and cancellation of vorticity. These mechanisms are shown to be related to the misalignment of the concentration gradient and the slip velocity, as well as to the difference in fluid and particle vorticities. Preliminary insight into the physics is obtained from an analysis of the unidirectional base flow. For this model problem, the conditions are established under which the particle velocity remains a single-valued function of space for all times. The resulting simplified set of two-way-coupled equations governing the vorticity of the fluid and particulate phases, respectively, is solved numerically. The formation of a decaying travelling wave solution is demonstrated over a wide range of parameters. Interestingly, the downward propagation of the fluid vorticity field is not accomplished through convection, but rather by the production and loss of vorticity on opposite sides of the mixing layer. For moderate settling velocities, the simulation results reveal an optimal coupling mechanism between the fluid and particle vorticities at intermediate values of the mass loading parameter. For large settling velocities and intermediate mass loadings, more than one local maximum is seen to evolve in the vorticity field. A scaling law for the downward propagation rates of the vorticity fronts is derived.

Two-dimensional particle-laden mixing layers are investigated by means of a mixed Lagrangian–Eulerian approach which is based on the vorticity variable. For uniformly seeded mixing layers, the simulations confirm some of the features observed by Druzhinin (1995*b*) for the model problem of a two-way-coupled particle-laden Stuart vortex, as well as by Dimas & Kiger (1998) in a linear stability analysis. For small values of the Stokes number, a mild destabilization of the mixing layer is observed. At moderate and large Stokes numbers, on the other hand, the transport of vorticity from the braids into the core of the evolving Kelvin–Helmholtz vortices is seen to be slowed by the two-way coupling effects. As a result, the particle ejection from the vortex cores is weakened. For constant mass loadings, the two-way coupling effects

---

† Author to whom correspondence should be addressed. Present address: Department of Mechanical and Environmental Engineering, University of California, Santa Barbara, CA 93106, USA, e-mail: meiburg@engineering.ucsb.edu

are strongest at intermediate Stokes number values. For moderately large Stokes numbers, the formation of two bands of high particle concentration is observed in the braids, which reflects the multi-valued nature of the particle velocity field. For mixing layers in which only one stream is seeded, the particle concentration gradient across the mixing layer leads to strong vorticity production and loss, which results in an effective net motion of the vortex in the flow direction of the seeded stream. Under particle settling, the vortex propagates downward as well. For the parameter range explored here, its settling velocity agrees well with the scaling law derived from the unidirectional flow analysis.

1. Introduction

Over the last decade, much insight into the evolution of particle-laden flows has been gained on the basis of one-way-coupled numerical simulations, which are based on formulations of the governing equations in which the fluid flow is not affected by the particle motion. As an example, numerous investigations of this kind for transitional free shear flows have shed light on the mechanisms that result in the preferential dispersion of particles whose aerodynamic response time is comparable to the characteristic time scale of the flow (Crowe, Gore & Troutt 1985; Chein & Chung 1988; Chung & Troutt 1988; Aggarwal & Xiao 1994; Uthuppan *et al.* 1994; Martin & Meiburg 1994; Raju & Meiburg 1995; Marcu & Meiburg 1996*a*; Ling *et al.* 1998; Soteriou & Yang 1999). Additional detailed studies have addressed such issues as particle accumulation due to inertial effects and during settling, as well as the formation of concentration waves in simplified models of particle-laden flows (Maxey 1987, 1990; Ganan-Calvo & Lasheras 1991; Tio *et al.* 1993*b*; Tio, Ganan-Calvo & Lasheras 1993*a*; Druzhinin 1994, 1995*a*, 1997; Marcu, Meiburg & Newton 1995; Marcu, Meiburg & Raju 1996; Marcu & Meiburg 1996*b*; Raju & Meiburg 1997). Statistical aspects of particle dispersion by fully turbulent flows have been the focus of several numerical investigations as well (Wang & Maxey 1993; Reeks 1991, 1992; Hyland, McKee & Reeks 1999; Elghobashi & Truesdell 1992).

As the mass loading of the particle phase increases, it can substantially alter the evolution of the fluid flow, so that an approach based on one-way coupling only is no longer appropriate. The effects of two-way coupling on the statistical properties of both isotropic and homogenous turbulence have been addressed in the numerical simulations of several authors (Squires & Eaton 1990; Elghobashi & Truesdell 1993; Truesdell & Elghobashi 1994; Maxey *et al.* 1997; Sundaram & Collins 1999), while other investigators have focused on the modification of wall turbulence (Pan & Banerjee 1996) and fully developed channel flows (Kulick, Fessler & Eaton 1994) by heavy particles. However, very little numerical work has been done regarding the effects of particle loading on the nonlinear stages of *transitional* free shear flows. Hence, a detailed understanding of the mechanisms by which the particulate phase affects the underlying vorticity dynamics of such flow fields has not yet been achieved, which renders the design of strategies for their optimization and control difficult. However, some preliminary insight can be gained from investigations of two-way-coupled model problems. Along these lines, Druzhinin (1995*b*) conducts an analysis of two-way coupling effects in several simplified flow fields such as free stagnation points, as well as constant vorticity and Stuart vortices, in order to obtain improved physical insight. By using a small Stokes number expansion, he makes the interesting

observation that two-way coupling effects lead to a reduction in the vorticity near vortex centres, while the strain is enhanced at hyperbolic free stagnation points. Qualitative modifications of the vorticity field by solid particles were furthermore observed by Park, Aggarwal & Katta (1996), as well as by Ory, Joia & Perkins (1998) for more complex flow fields.

In contrast to the nonlinear stages, the question of how the linear stability of shear flows is affected by a particulate phase has been the subject of several theoretical studies. An early analytical investigation of steady laminar flow involving two-way coupling effects was carried out by Saffman (1961). He observes fine particles, with a fairly small relaxation time relative to the characteristic time scale of the fluid flow, to destabilize the fluid motion. Conversely, coarser particles, with a greater relaxation time, act in a stabilizing fashion. In his analysis, the particle concentration is assumed to be constant everywhere in the flow field. Chen & Chung (1995) confirm these findings for oscillatory two-phase channel flow by numerically solving a linearized stability equation in the limit of very small particles. The stability of two-way-coupled particle-laden mixing layers was first addressed by Yang *et al.* (1990). Their linear stability analysis, which neglects the particle response to flow fluctuations, reveals the stabilizing effect of particles on the spatial and temporal instabilities of a *tanh* shear layer. Wen & Evans (1994) focus on the effects of differential particle loading on the stability of the mixing layer. Assuming unresponsive particles, their linear stability analysis shows two coexisting unstable modes, one of which is the Kelvin–Helmholtz mode. The second mode is found to be similar to the Holmboe instability observed in density-stratified flows, cf. the work by Lawrence, Browand & Redekopp (1991). Very recently, Dimas & Kiger (1998) extended the above linear stability analyses by retaining particle dynamics. Their detailed investigation focuses on the impact of the particle Stokes number and the mass loading, and they observe that an increase in either one of these parameters decreases the growth rate of the instability. Under certain conditions, they find the appearance of a second, low-frequency instability mode in addition to the fundamental mode. Their results show the velocity, particle concentration, and vorticity fields to be strongly coupled.

It needs to be pointed out that several experimental investigations as well have addressed specifically the effects of particle feedback on the flow. For a particle-laden free jet, Fleckhaus, Hishida & Maeda (1987) show that a fairly low mass loading of 30% has a considerable effect on the properties of the jet. Their laser velocimetry experiments indicate that the centreline air velocity declines at a rate somewhat lower than that of the corresponding single-phase jet. Kiger & Lasheras (1995) analyse the kinetic energy transfer between the two phases in a droplet-laden mixing layer. The same authors (Kiger & Lasheras 1997) find that the dissipation in a two-phase turbulent mixing layer increases due to the particles' presence. To our knowledge, experimental data on the effects of the particulate phase on the growth rate and/or phase velocity of the Kelvin–Helmholtz instability in a mixing layer are not at present available.

Efforts to obtain a deeper understanding of the two-way coupling mechanisms that dominate the nonlinear stages of transitional flows require accurate numerical simulations that properly account for the underlying physics. Towards this end, over the last two decades several computational approaches have been developed for the modelling of two-way coupling effects in relatively dilute two-phase flows. In his review of flows with a moderate mass loading, Sirignano (1993) lucidly describes how one can base such investigations on two-continua formulations, Lagrangian discrete particle approaches, and probabilistic descriptions. He furthermore discusses various considerations that, for a given application, may render one of these approaches preferable

to the others. A detailed and thorough overview of the continuum formulations is provided by Drew (1983). However, for investigations of some of the fundamental physics of particle-laden two-phase flows, in recent years the preferred computational approach appears to have been Lagrangian in nature, cf. also the recent review of numerical models by Crowe, Troutt & Chung (1996). Such simulations typically track many discrete particles individually on the basis of an equation that balances the various forces acting on each of the particles. Since these particles do not interact which each other, they are usually allowed to overlap spatially. Of interest with regard to the numerical aspects of the present investigation is the advantage of the Lagrangian approach that it does not require the particle velocity to be a single-valued function of space. In other words, particles that occupy the same spatial volume element are not required to have the same velocity values. The assumption of single-valuedness is usually made implicitly when continuum approaches are employed that discretize the physical space only. However, the effects of particle inertia in general prevent the particle velocity from being such a single-valued function of space, except for very small values of the Stokes number. In the literature, this is sometimes referred to as the 'crossing trajectories effect', which is a somewhat misleading term, as particle trajectories can cross even for single-valued particle velocities, as long as the problem is unsteady in nature. Strictly speaking, if inertial effects are significant, a continuum equation for the particle concentration in physical space has to be formulated based on the particle distribution function in phase space, cf. for example the spray equation discussed in detail by Williams (1985). This approach is referred to as the probabilistic formulation by Sirignano (1993). However, simulations that require the discretization of the phase space are exceedingly expensive computationally due to the increased dimensionality of the problem, so that this approach in the past has not been considered practical for simulating multidimensional flow fields. As a result, phase-space dynamics have mainly been considered in order to derive lower-dimensional models suitable for the physical space.

In the present investigation, we will examine more closely the conditions under which the particle velocity field in the *unidirectional* base flow of a mixing layer remains single-valued. The equations governing the two-way-coupled fluid and particle motion under these circumstances will be derived, and numerical solutions for a variety of parameter combinations will be presented, in order to gain further insight into the two-way coupling effects. Subsequently, the focus will be on the computational simulation of nonlinearly evolving, *two-dimensional* two-way-coupled mixing layers. As we will see, for larger values of the Stokes number, the particle velocities usually are not single-valued. Since our interest covers the entire range of Stokes number values, a single-valued particle velocity field thus cannot be assumed. Instead, a Lagrangian particle tracking approach will be employed in order to examine in some detail the relevant mechanisms by which the particulate phase affects the nonlinear time-dependent evolution of the fluid motion. In particular, our interest will focus on the modifications due to two-way coupling of the well-known particle ejection process from the vortex cores and the related formation of high-concentration particle streaks in the braids. One-way-coupled investigations had identified these mechanisms as crucial ingredients in the dispersion process.

Throughout this investigation, the importance of the vorticity variable, and of the ways in which it is affected by the two-way coupling, will be emphasized, in order to develop a vorticity-based interpretation of the two-way coupling mechanisms in free shear flows. While the present work is limited to two dimensions, the ultimate goal is to obtain an understanding of how the production and cancellation of vorticity through

two-way coupling processes affects and alters the convection, diffusion, and stretching of this variable, i.e. the mechanisms that are known to govern the evolution of single-phase free shear flows. Employing a vorticity formulation in the investigation of two-way-coupled two-phase flows presents certain numerical challenges, as will be seen in detail below. These result mostly from the requirement to obtain spatial derivatives of the coupling forces, which translates into the need to have a differentiable particle number density field. To this end, a combined Lagrangian–Eulerian numerical method will be introduced, the novel features of which will be discussed in detail.

The paper is organized as follows. Section 2 states the equations that govern the particle distribution function in phase space and, for single-valued particle velocity fields, the particle concentration in physical space. The relevant dimensionless parameters are identified, and the two-way coupling between fluid and particles via the momentum equation is formulated. The two-way-coupled equations for the fluid motion are given in the vorticity formulation, and the physical mechanisms that lead to the production and loss of vorticity are discussed. In §3, the temporal evolution of a two-way-coupled unidirectional mixing layer flow is addressed. The conditions under which the particle velocity remains a single-valued function of space are derived. The resulting equations are solved, the influence of the respective governing parameters is discussed, and scaling laws are formulated. Subsequently, §4 describes the combined Lagrangian-Eulerian approach in some detail. In §5 results are presented for both uniformly and differentially loaded two-dimensional two-way-coupled mixing layers, with and without the effects of gravity. Finally, §6 will present a brief summary and draw several conclusions.

2. Governing equations

2.1. *Conservation equation for the particulate phase*

The present investigation addresses the effects of two-way coupling mechanisms on time-dependent, viscous flows containing a dilute distribution of small, heavy, monodisperse, spherical particles or droplets. In the following, we limit ourselves to situations in which interactions among these particles are negligible and their size does not change with time due to effects such as, for example, condensation or evaporation. For an overview over these important effects, the reader is referred to the review by Sirignano (1993) and the extensive references provided therein. Under these conditions, the particle distribution function $f(x, u_p, t)$ in phase space, where u_p denotes the particle velocity vector, is governed by the Boltzmann-like spray equation (Williams 1985)

$$\frac{\partial f}{\partial t} = -\nabla_x \cdot (u_p f) - \nabla_{u_p} \cdot (a_p f), \tag{2.1}$$

where, for two-dimensional flow,

$$\nabla_x = (\partial/\partial x, \partial/\partial y)^T, \tag{2.2a}$$

$$\nabla_{u_p} = (\partial/\partial u_p, \partial/\partial v_p)^T, \tag{2.2b}$$

$$a_p = \frac{\mathrm{d}u_p}{\mathrm{d}t}, \tag{2.2c}$$

$$u_p = \frac{\mathrm{d}x_p}{\mathrm{d}t}. \tag{2.2d}$$

Here, $\boldsymbol{x}_p$ and $\boldsymbol{a}_p(\boldsymbol{x}_p, \boldsymbol{u}_p, t)$ denote the particle location and acceleration, respectively. The particle number density $n(\boldsymbol{x}, t)$ in physical space is related to the distribution function in phase space by

$$n(\boldsymbol{x}, t) = \int_{-\infty}^{\infty} f(\boldsymbol{x}, \boldsymbol{u}_p, t) \mathrm{d}\boldsymbol{u}_p. \tag{2.3}$$

In a dilute, particle- or droplet-laden flow such as a spray or an aerosol, the particle acceleration $\boldsymbol{a}_p$ can be related to the instantaneous local particle and fluid velocities by considering the forces acting on an isolated spherical particle, cf. Williams (1985). For the case of particles that are much smaller than the characteristic length scales of the velocity field, a corresponding equation of motion, expressing a balance of these forces, was formulated by Maxey & Riley (1983). The history term contained in this equation, whose formulation dates back to Basset, has been under some scrutiny since, see the recent work by Kim, Elghobashi & Sirignano (1998), as well as references therein. However, our interest focuses on situations in which the density of the particle material is much greater than that of the fluid. Under such conditions, the history term becomes negligible, along with the forces due to virtual mass and pressure gradients, compared to the contribution of the viscous drag and gravity, cf. the order of magnitude analysis conducted by Lazaro & Lasheras (1989). By furthermore assuming Stokes flow around the particles, we obtain

$$\boldsymbol{a}_p \equiv \frac{\mathrm{d}\boldsymbol{u}_p}{\mathrm{d}t} = \frac{3\pi\mu d_p}{m_p}[\boldsymbol{u}(\boldsymbol{x}_p) - \boldsymbol{u}_p] - g\boldsymbol{e}_y. \tag{2.4}$$

This equation expresses the balance of particle inertia, viscous drag, and gravity. m_p represents the particle mass, μ denotes the dynamic fluid viscosity, and d_p is the particle diameter. $\boldsymbol{u}(\boldsymbol{x}_p)$ denotes the fluid velocity at the particle location, and g is the strength of the gravitational acceleration, which points in the $-y$-direction.

The above equations for the particle distribution function (2.1) and the particle acceleration (2.4) are rendered dimensionless by introducing characteristic scales for the value of the distribution function, as well as velocity, length, and particle number density, respectively:

$$f^* = F, \qquad u^* = U, \qquad l^* = L, \qquad n^* = N. \tag{2.5}$$

For the specific case of a temporally growing, spatially periodic mixing layer to be considered below, U represents the velocity difference across the shear layer, L denotes its width at the initial time of the simulation, and N is the nominal particle number density in the seeded stream. In this way, we obtain for a two-dimensional flow

$$\frac{\partial f}{\partial t} = -\nabla_{\boldsymbol{x}} \cdot (\boldsymbol{u}_p f) - \frac{1}{St}\nabla_{\boldsymbol{u}_p} \cdot [(\boldsymbol{u} - \boldsymbol{u}_p)f] + \frac{1}{Fr^2}\frac{\partial f}{\partial v_p}, \tag{2.6a}$$

$$\frac{\mathrm{d}\boldsymbol{u}_p}{\mathrm{d}t} = \frac{1}{St}(\boldsymbol{u} - \boldsymbol{u}_p) - \frac{\boldsymbol{e}_y}{Fr^2}, \tag{2.6b}$$

$$\frac{\mathrm{d}\boldsymbol{x}_p}{\mathrm{d}t} = \boldsymbol{u}_p, \tag{2.6c}$$

where $\boldsymbol{e}_y$ is the unit vector in the y-direction. As the governing parameters, we identify the Stokes number St and the Froude number Fr:

$$St = \frac{\tau_p}{\tau_f}, \quad Fr = \frac{U}{\sqrt{Lg}}. \tag{2.7}$$

Here the fluid time scale τ_f and the particle aerodynamic response time τ_p are defined as $\tau_f = L/U$ and $\tau_p = d_p^2 \rho_p / 18\mu$, respectively, where ρ_p indicates the density of the particle material. τ_p can be viewed as a measure of the responsiveness of a particle to a change in the fluid velocity field, while τ_f gives an indication of the time available for the interaction of the particle with the large-scale structures, cf. Chein & Chung (1988). *Fr* measures the importance of gravitational forces.

When integrating over the u_p- and v_p-directions of the phase space, the last three terms on the right-hand side of equation (2.6a) vanish, and the following relationship for the particle number density results:

$$\frac{\partial n}{\partial t} = -\int_{-\infty}^{\infty} \nabla_x \cdot (\boldsymbol{u}_p f) \mathrm{d}\boldsymbol{u}_p. \tag{2.8}$$

In general, the above integrals will have to be evaluated numerically in phase space, which leads to the costly higher dimensionality of the problem mentioned in the introduction. However, when u_p and v_p are single-valued functions of the spatial location x, i.e., $\boldsymbol{u}_p = \boldsymbol{u}_p(\boldsymbol{x}, t)$, we obtain

$$\int_{-\infty}^{\infty}\int_{-\infty}^{\infty} \frac{\partial}{\partial x}(u_p f) \,\mathrm{d}u_p\,\mathrm{d}v_p = \frac{\partial}{\partial x}\left[u_p \int_{-\infty}^{\infty}\int_{-\infty}^{\infty} f\,\mathrm{d}u_p\,\mathrm{d}v_p\right] = \frac{\partial}{\partial x}(u_p n), \tag{2.9a}$$

$$\int_{-\infty}^{\infty}\int_{-\infty}^{\infty} \frac{\partial}{\partial y}(v_p f) \,\mathrm{d}u_p\,\mathrm{d}v_p = \frac{\partial}{\partial y}\left[v_p \int_{-\infty}^{\infty}\int_{-\infty}^{\infty} f\,\mathrm{d}u_p\,\mathrm{d}v_p\right] = \frac{\partial}{\partial y}(v_p n). \tag{2.9b}$$

As a consequence, the equation for the particle number density takes the form

$$\frac{\partial n}{\partial t} = -\nabla_x \cdot (\boldsymbol{u}_p n). \tag{2.10}$$

This demonstrates that a lower-dimensional problem results if the particle velocity is a single-valued function of space. Below, we will investigate in some detail the conditions under which the unidirectional base flow of a particle-laden mixing layer satisfies this prerequisite. In general, however, inertial effects will render the particle velocity a multi-valued function of space, and numerical simulations will either have to be based on the higher-dimensional conservation equation for the particle distribution function in phase space, or on a Lagrangian approach along the lines described below in §4.

2.2. *Two-way coupling via the momentum equation*

Depending on the parameter regime, different approaches to accounting for two-way coupling effects are most suitable. An overview over these various approaches is provided by Sinclair (1997), as well as Crowe, Sommerfeld & Tsuji (1998). For dilute suspensions of particles that are small enough for their inertia to be negligible, the most convenient model employs a single-phase Boussinesq fluid, whose density depends on the local particle concentration. The particulate phase can then be described by a convection–diffusion equation for its concentration, which can also account for uniform gravitational settling. Such a model has been applied, for example, by Härtel *et al.* (1999) in their investigation of particle-driven gravity currents.

If, on the other hand, particle inertia is important, the momentum coupling between particle and fluid motion can be approximated most straightforwardly by assuming that each particle locally exerts a force on the fluid that is opposite and equal to the force experienced by the particle, cf. Williams (1985), as well as the more recent numerical applications by Squires & Eaton (1990), Elghobashi & Truesdell (1993),

Maxey *et al.* (1997), as well as Wallner & Meiburg (1998). In order to determine the collective force density l with which the particles located in a differential control volume act on the fluid, one defines the average particle velocity $\bar{u}_p(x, t)$ in the differential control volume

$$\bar{u}_p = \frac{1}{n} \int_{-\infty}^{\infty} f u_p \, \mathrm{d}u_p. \tag{2.11}$$

Assuming a Stokes drag force, one thus obtains the dimensional relationship

$$l = n3\pi\mu d_p(\bar{u}_p - u). \tag{2.12}$$

In focusing on the coupling mechanisms of dilute particle- or droplet-laden flows, we neglect the volume fraction of the particle phase in the continuity equation for the fluid. This approximation is valid when investigating, for example, the dynamics of sprays or aerosols, where for typical mass loadings of $O(1)$ the volume fraction of the particulate phase is of $O(10^{-3})$. The mass and momentum equations governing the constant-density fluid motion thus take the form

$$\nabla \cdot u = 0, \tag{2.13a}$$

$$\rho\frac{\partial u}{\partial t} + \rho(u \cdot \nabla)u = -\nabla p + \mu\nabla^2 u + n3\pi\mu d_p(\bar{u}_p - u). \tag{2.13b}$$

Upon non-dimensionalization, we obtain

$$\nabla \cdot u = 0, \tag{2.14a}$$

$$\frac{\partial u}{\partial t} + (u \cdot \nabla)u = -\nabla p + \frac{1}{Re}\nabla^2 u + n\frac{D}{St}(\bar{u}_p - u). \tag{2.14b}$$

Here the Reynolds number Re and the dimensionless mass loading D, respectively, are defined as

$$Re = \frac{UL}{\nu}, \quad D = \frac{\bar{\rho}_p}{\rho}, \tag{2.15}$$

where

$$\bar{\rho}_p = m_p N \tag{2.16}$$

denotes the nominal mass of particle material per unit volume of the flow in the seeded stream.

As mentioned earlier, the present investigation ultimately aims at understanding the two-way coupling effects, as well as the related production and loss of vorticity, in terms of their ability to modify the balance of convection, diffusion, and, in three dimensions, stretching of vorticity. Formulated differently, our goal is to identify the routes by which the two-way coupling effects can alter the mechanisms known to govern the vorticity dynamics of single-phase free shear flows. Regarding the linear aspects of this issue, Dimas & Kiger (1998) interpret their theoretical stability results from a vorticity-based point of view. They find that modifications of the vorticity field are due to the divergence of the particle velocity field. It is instructive to formulate the conservation equations for the fluid motion in terms of the vorticity variable ω, cf. Druzhinin (1995b). For the present situation of two-dimensional flows, additional benefits are realized by employing the streamfunction ψ, which results in

$$\frac{\partial \omega}{\partial t} + (u \cdot \nabla)\omega = \frac{1}{Re}\nabla^2\omega + \frac{D}{St}\nabla \times [n(\bar{u}_p - u)] \cdot e_z, \tag{2.17a}$$

$$\nabla^2\psi = -\omega, \tag{2.17b}$$

$$u = \frac{\partial \psi}{\partial y}, \quad (2.17c)$$

$$v = -\frac{\partial \psi}{\partial x}. \quad (2.17d)$$

Equation (2.17a) allows us to readily identify the physical mechanisms by which the particulate phase will affect the evolution of the vorticity field. We recognize that the presence of the particulate phase manifests itself as a source term, which indicates the local production or destruction (cancellation) of vorticity. For the specific example of a mixing layer, the spatio-temporal distribution of this source term will then determine the extent to which the interplay of vorticity convection and diffusion, which governs the evolution of the Kelvin–Helmholtz instability, is modified by the presence of the particulate phase, and whether these modifications will result in the amplification or damping of the instability. The magnitude of the source term depends both on the mass loading as well as on the particle Stokes number. Spatial variations in the particle number density field in combination with a local velocity difference (slip velocity) between the two phases are seen to result in the production or loss of vorticity. Based on the above vorticity equation, it is reasonable to expect larger mass loadings D to result in stronger two-way coupling effects. On the other hand, interpreting the influence of St requires more caution, as this parameter also appears in the particle equation of motion, where it directly affects the slip velocity.

In order to gain some preliminary insight into the fundamental nature of the coupling mechanisms, and how they affect the vorticity field, we will first focus on the evolution of the unperturbed, unidirectional base flow laden with monodisperse particles, and under the effect of gravity. An investigation along similar lines has been conducted by Katoshevski & Tambour (1993). However, while these authors neglect the effect of gravity, they do allow for evaporating, polydisperse droplets. A comparsion of their theoretical results with the experimental observations of Lazaro & Lasheras (1989, 1992*a, b*) for sprays impressively demonstrates the usefulness of considering such simplified flow models.

3. Temporal evolution of the unidirectional base flow in the absence of perturbations

Consider the case in which the fluid velocity initially is given by the unidirectional, horizontal base flow

$$\boldsymbol{u}(y, t = 0) = (0.5 \tanh y, 0)^T. \quad (3.1)$$

Let us furthermore assume that the initial conditions for the particle velocity $\boldsymbol{u}_p$ and number density n are independent of x as well. Then, in the absence of two-dimensional perturbations, we obtain for all times

$$\frac{\partial}{\partial x}(u, \boldsymbol{u}_p, n) \equiv 0, \quad v(\boldsymbol{x}, t) \equiv 0. \quad (3.2)$$

Even though the above fluid flow remains strictly unidirectional for all times, a non-trivial dynamical evolution will develop as a result of the time-dependent coupling between the fluid and the particle motion, since both the settling of the particles as well as the viscous diffusion of the streamwise fluid momentum will maintain the presence of slip velocities. The equations of motion governing this unidirectional,

two-way-coupled base flow take a particularly simple form if the particle velocity field remains a single-valued function of space for all times. In the following, we will establish the conditions for which this is the case.

3.1. *Conditions under which the particle velocity field remains a single-valued function of space for all times*

For the above unidirectional flow, it is of interest to establish the conditions under which a particle velocity field that initially represents a single-valued function of space will maintain this property for all times. This will be the case if particles that are released at different initial y-locations y_{p0}, possibly with different initial vertical velocities $v_{p0}(y_{p0})$, continue to occupy different y-locations for all times. We can express the y-location of a particle as a function of its release location and time as $h(y_{p0}, t)$:

$$h(y_{p0}, t) = y_{p0} + \int_0^t v_p(y_{p0}, t)\mathrm{d}t, \tag{3.3}$$

where $v_p(y_{p0}, t)$ denotes the Lagrangian, time-dependent vertical velocity of the particle released at y_{p0}. We thus obtain as condition for single-valuedness

$$\frac{\partial h}{\partial y_{p0}}(y_{p0}, t) > 0. \tag{3.4}$$

In other words, if particle 2 starts at a higher (lower) y-location than particle 1, its y-location will have to remain higher (lower) than that of particle 1 for all times. For vanishing vertical fluid velocity, equation (2.6*b*) states that $v_p(y_{p0}, t)$ is governed by

$$\frac{\partial v_p}{\partial t} = -\frac{1}{St}v_p - \frac{1}{Fr^2}, \tag{3.5}$$

which has the solution

$$v_p(y_{p0}, t) = \left[v_{p0}(y_{p0}) + \frac{St}{Fr^2}\right]\mathrm{e}^{-t/St} - \frac{St}{Fr^2}. \tag{3.6}$$

Here St/Fr^2 is the dimensionless terminal settling velocity. Substitution of this result into equation (3.3) yields

$$\frac{\partial h}{\partial y_{p0}}(y_{p0}, t) = 1 + \frac{\mathrm{d}v_{p0}}{\mathrm{d}y_{p0}}St(1 - \mathrm{e}^{-t/St}). \tag{3.7}$$

Thus, for $\mathrm{d}v_{p0}/\mathrm{d}y_{p0} \geqslant 0$, condition (3.4) is always satisfied. On the other hand, if $\mathrm{d}v_{p0}/\mathrm{d}y_{p0} < 0$, we must require

$$\frac{\mathrm{d}v_{p0}}{\mathrm{d}y_{p0}} > -\frac{1}{St}. \tag{3.8}$$

This indicates that the rate at which the vertical release velocity of the particles drops off with y is not allowed to exceed a certain value if the particle velocity is to remain a single-valued function of y for all times. Furthermore, note that whether or not v_p remains a single-valued function of space it depends neither on the horizontal release velocity nor on the mass loading. In the following, we will focus on the special case in which the particles are released everywhere with the local fluid velocity, i.e.

$$\boldsymbol{u}_{p0}(y_{p0}) = \boldsymbol{u}(y_{p0}, t = 0). \tag{3.9}$$

3.2. *The case of particles being released with the fluid velocity*

Since v_p stays independent of y for all times, the spray equation (2.6a) now takes the form

$$\frac{\partial f}{\partial t} = -v_p \frac{\partial f}{\partial y} - \frac{1}{St}\frac{\partial}{\partial u_p}[(u - u_p)f] + \frac{1}{St}\frac{\partial}{\partial v_p}(v_p f) + \frac{1}{Fr^2}\frac{\partial f}{\partial v_p}. \tag{3.10}$$

By integrating this equation over the u_p- and v_p-directions, a lower-dimensional differential equation for the particle number concentration n in physical space is thus obtained as

$$\frac{\partial n}{\partial t} = -v_p(t)\frac{\partial n}{\partial y}. \tag{3.11}$$

For the particular initial condition of

$$n(y, t = 0) = n_0, \tag{3.12}$$

we recognize that the particle number concentration field does not depend on space or time. As a further consequence of the single-valued nature of the particle velocity field, we can define a particle vorticity

$$\omega_p(y, t) = -\frac{\partial u_p}{\partial y}. \tag{3.13}$$

The horizontal particle velocity is then governed by

$$\frac{\mathrm{d}u_p}{\mathrm{d}t} = \frac{\partial u_p}{\partial t} + v_p \frac{\partial u_p}{\partial y} \tag{3.14a}$$

$$= \frac{\partial u_p}{\partial t} - v_p \omega_p, \tag{3.14b}$$

where $\mathrm{d}/\mathrm{d}t$, as before, denotes the Lagrangian derivative following the particle motion. For the present case of $v_{p0}(y) = 0$, we thus obtain with equations (3.6) and (2.6b)

$$\frac{\partial u_p}{\partial t} + \frac{St}{Fr^2}(1 - \mathrm{e}^{-t/St})\omega_p = \frac{1}{St}(u - u_p), \tag{3.15}$$

and, by taking $\partial/\partial y$,

$$\frac{\partial \omega_p}{\partial t} - \frac{St}{Fr^2}(1 - \mathrm{e}^{-t/St})\frac{\partial \omega_p}{\partial y} = \frac{1}{St}(\omega - \omega_p). \tag{3.16}$$

The evolution of the fluid and particle vorticities is thus described by the relatively simple system of coupled partial differential equations

$$\frac{\partial \omega}{\partial t} = \frac{1}{Re}\frac{\partial \omega}{\partial y^2} + \frac{D}{St}(\omega_p - \omega), \tag{3.17a}$$

$$\frac{\partial \omega_p}{\partial t} = \frac{St}{Fr^2}(1 - \mathrm{e}^{-t/St})\frac{\partial \omega_p}{\partial y} + \frac{1}{St}(\omega - \omega_p), \tag{3.17b}$$

subject to the initial and boundary conditions

$$\omega(y, 0) = \omega_p(y, 0) = -\frac{1}{2\cosh^2(y)}, \tag{3.18a}$$

$$\omega(y \to \pm\infty, t) = \omega_p(y \to \pm\infty, t) = 0. \tag{3.18b}$$

For this particular flow, the four independent parameters (Re, D, St, and Fr) can be reduced to three by rescaling time as

$$t^* = \frac{t}{St}. \tag{3.19}$$

In this way, we obtain

$$\frac{\partial \omega}{\partial t^*} = \frac{St}{Re}\frac{\partial \omega}{\partial y^2} + D(\omega_p - \omega), \tag{3.20a}$$

$$\frac{\partial \omega_p}{\partial t^*} = \frac{St^2}{Fr^2}(1 - e^{-t^*})\frac{\partial \omega_p}{\partial y} + (\omega - \omega_p). \tag{3.20b}$$

This rescaled problem is thus governed by the three dimensionless parameters

$$D, \quad \frac{St}{Re}, \quad \frac{St^2}{Fr^2}, \tag{3.21}$$

which can be interpreted as the mass loading factor, a rescaled Reynolds number, and a rescaled settling velocity.

3.3. *Numerical results for the two-way-coupled unidirectional base flow*

The above coupled system (3.20a), (3.20b) can be solved numerically in a straightforward fashion by any of a number of standard methods. In the present investigation, we opt for a finite difference scheme of Crank–Nicolson type, which is of second order both in space and in time. The grid spacing Δy is typically taken to be 0.05. Since the effective convection velocities and diffusion coefficients in equations (3.20a) and (3.20b) depend on the values of the governing parameters, the size of the time step Δt has to be adjusted accordingly. Along similar lines, computational domains of different size are employed for different parameter combinations.

In the following, we will separately evaluate the influence of the governing dimensionless parameters D and St^2/Fr^2 on the spatio-temporal evolution of the fluid and particle vorticities. Particular emphasis will be placed on the strength of the coupling between the two phases, as well as on how this coupling affects the rates at which the two respective vorticity peaks decay and propagate downward. Here, it is important to realize that the particle settling velocity $v_p(t^*)$ is given by

$$v_p(t^*) = \frac{St^2}{Fr^2}(e^{-t^*} - 1) \tag{3.22}$$

and does not depend on the spatial location y, on D, or on St/Re.

Furthermore, several globally conserved quantities can be identified. Since far below and far above the mixing layer, both the fluid and the particle velocities in the x-direction for all times will asymptotically approach the values of -0.5 and 0.5, respectively, we have

$$\int_{-\infty}^{\infty} \omega(y, t^*)\mathrm{d}y = \int_{-\infty}^{\infty} \omega_p(y, t^*)\mathrm{d}y = -1, \tag{3.23}$$

i.e. the global fluid and particle circulations are equal and constant in time. At first glance, this may seem at odds with the fact that the respective production terms in the equations for ω and ω_p, while being of opposite signs, differ by a factor of D in magnitude. However, this apparent contradiction is resolved by realizing that, in each
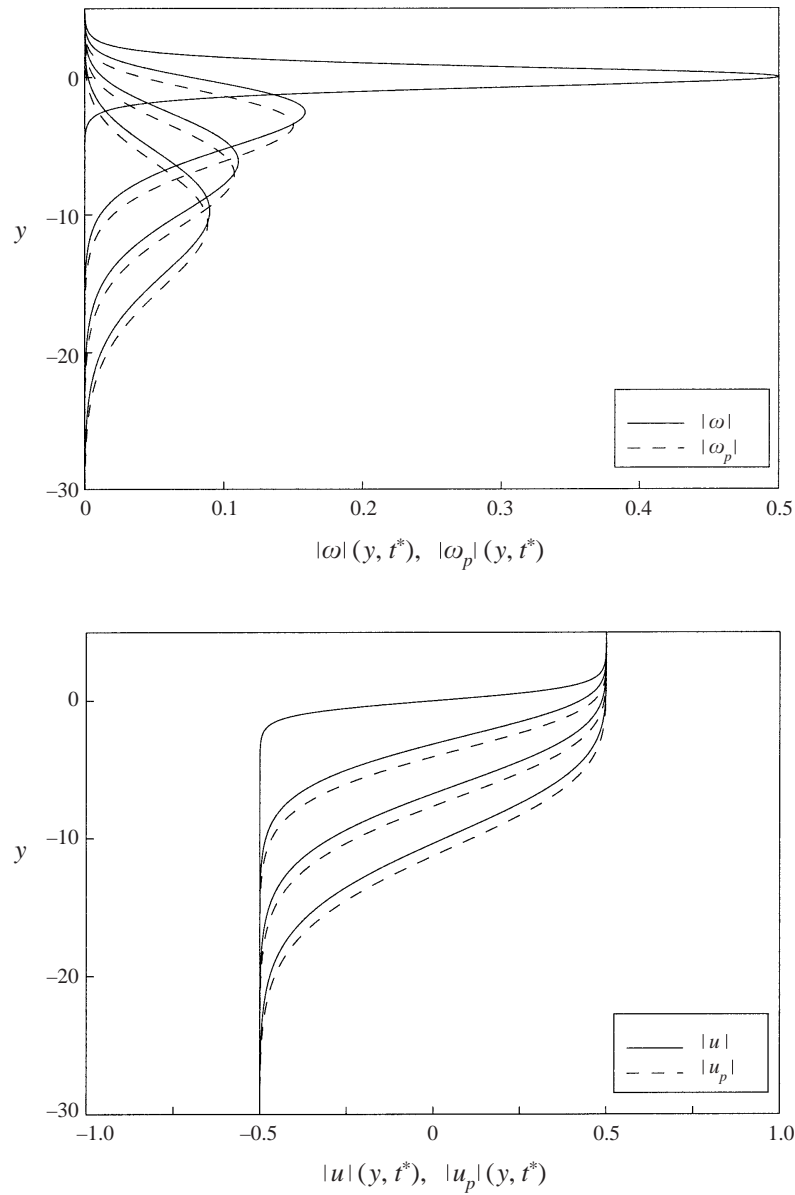
FIGURE 1. Particle and fluid vorticity and velocity profiles as function of time for $D = 0.1$, $St^2/Fr^2 = 1$, $St/Re = 0.01$ and times 0, 40, 80 and 120. The production and cancellation of vorticity leads to an effective downward migration of the fluid and particle vorticity and velocity profiles.

of the two vorticity equations *separately*, the integral across the mixing layer over the production term identically vanishes for all times

$$\int_{-\infty}^{\infty} [\omega_p(y,t^*) - \omega(y,t^*)]dy \equiv 0. \tag{3.24}$$

3.3.1. *Influence of the mass loading parameter D*

Inspection of equations (3.20a) and (3.20b) shows that the mass loading factor D represents the primary parameter responsible for two-way coupling effects, since

its magnitude determines the strength of the feedback from the particle motion to the fluid motion. A value of $D \ll 1$ might suggest this feedback to be fairly weak, so that one may expect the fluid motion to evolve in a fashion that is largely unaffected by the particulate phase. However, the feedback also depends on the magnitude of the vorticity difference, which will *increase* with time if the fluid motion develops independently of the particulate phase. A typical situation for $D \ll 1$ is shown in figure 1, for $D = 0.1$, $St^2/Fr^2 = 1$ and $St/Re = 0.01$. It is important to realize that the signs of the respective source terms in the vorticity equations are such that the settling of the particles leads to a cancellation of the fluid vorticity on the upper side of the shear layer, while additional fluid vorticity is produced on its lower side. In this way, the maximum of the fluid vorticity, while decaying as a result of diffusion, is shifted to lower y-values. It should be emphasized that this shift is unrelated to any convection of fluid ($v(y,t) \equiv 0$ everywhere), and due exclusively to the source term. For the same reason, the maximum of the particle vorticity is not convected downward along with the settling particles. Instead, the production and cancellation of particle vorticity due to the coupling with the fluid motion are distributed such that the particle vorticity maximum remains just below that of the fluid vorticity for all times. In summary, the respective source terms in the equations governing the fluid and particle vorticity have the effect of driving these two quantities towards each other. This effect is balanced by the settling of the particles, which tends to increase the local difference between the two vorticity fields.

This coupling of the vorticity fields can clearly be recognized in figure 2, which shows the values as well as the locations of the two vorticity maxima as a function of time. Initially, the location of the particle vorticity maximum rapidly propagates downward, without having much of an effect on the location of the fluid vorticity maximum. However, as soon as the difference $\omega - \omega_p$ becomes large enough, the coupling gets stronger, and for long times the two vorticity maxima propagate downward with identical velocities, in the form of a decaying travelling wave solution.

For $D \gg 1$, the situation is somewhat different, cf. figure 3. Here even small differences $\omega - \omega_p$ quickly drive the fluid vorticity towards the particle vorticity. Consequently, the coupling term in the particle vorticity equation will remain small for all times, so that the coupled vorticity profiles propagate downward with a velocity that is close to the particle settling velocity, cf. figure 4.

By comparing figures 2 and 4, one recognizes that for two-way-coupled flows the decay rate of the fluid vorticity maximum does not depend only on the diffusive effects, as expressed by the rescaled Reynolds number Re/St, but also on the mass loading ratio D. Figure 5 depicts the time evolution for several different D values. It is quite interesting to note that for $D \approx 1$, the coupling between the two phases is optimal in the sense that the maximum of the fluid vorticity decays much more rapidly than for either very large or very small values of D.

3.3.2. *Influence of the rescaled settling velocity St^2/Fr^2*

For a reduced settling velocity of $St^2/Fr^2 = 0.1$, the behaviour is quite similar to the case $St^2/Fr^2 = 1$ described above. However, for $St^2/Fr^2 = 10$, a set of different interesting dynamical features can be observed. At small mass loadings such as $D = 0.1$ (figure 6), the rapid settling of the particles leads to an effective decoupling of the fluid and particle vorticities during the early stages. The maximum of the particle vorticity is seen to quickly propagate downward without being able to set up a corresponding propagating front in the fluid vorticity profile. As a result, a
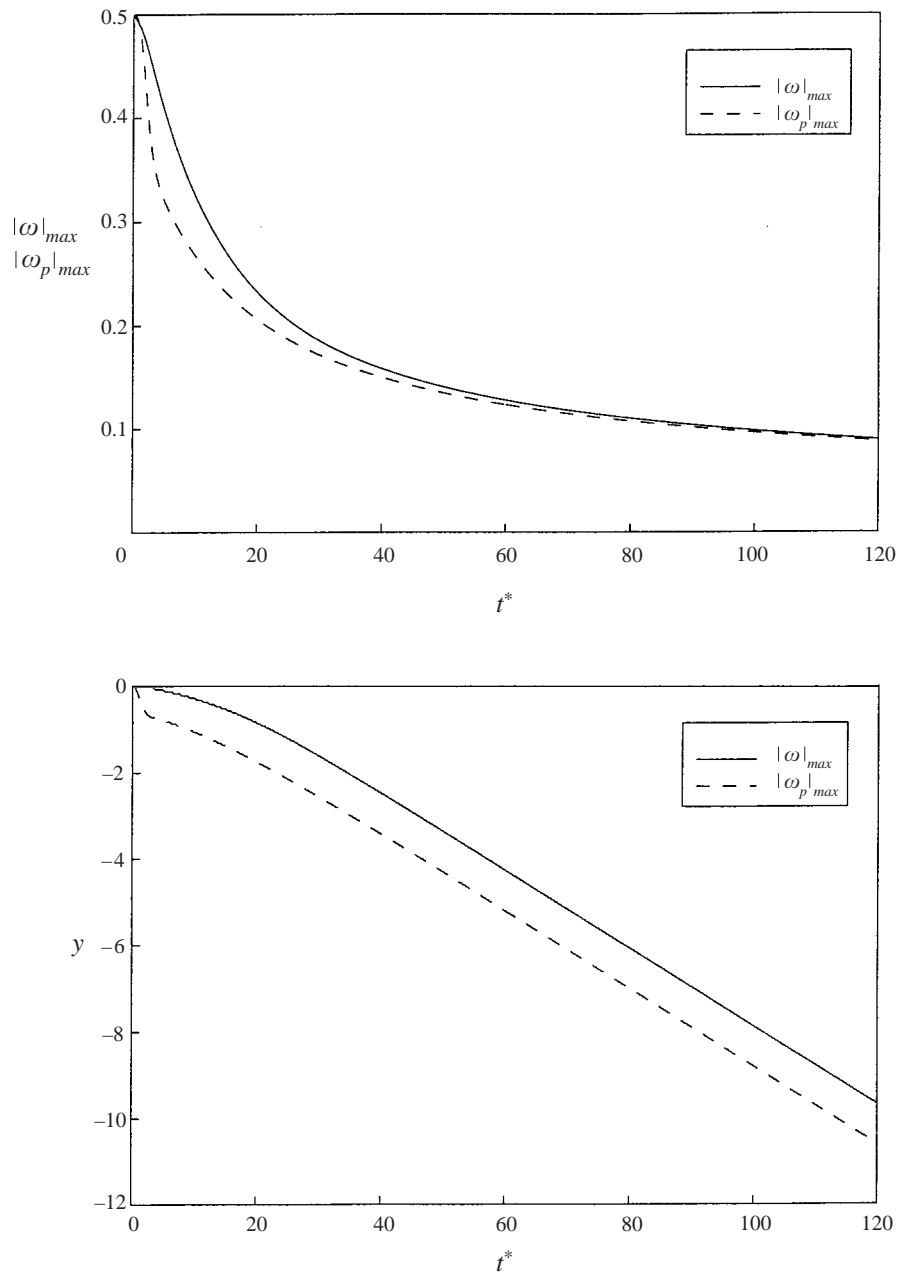
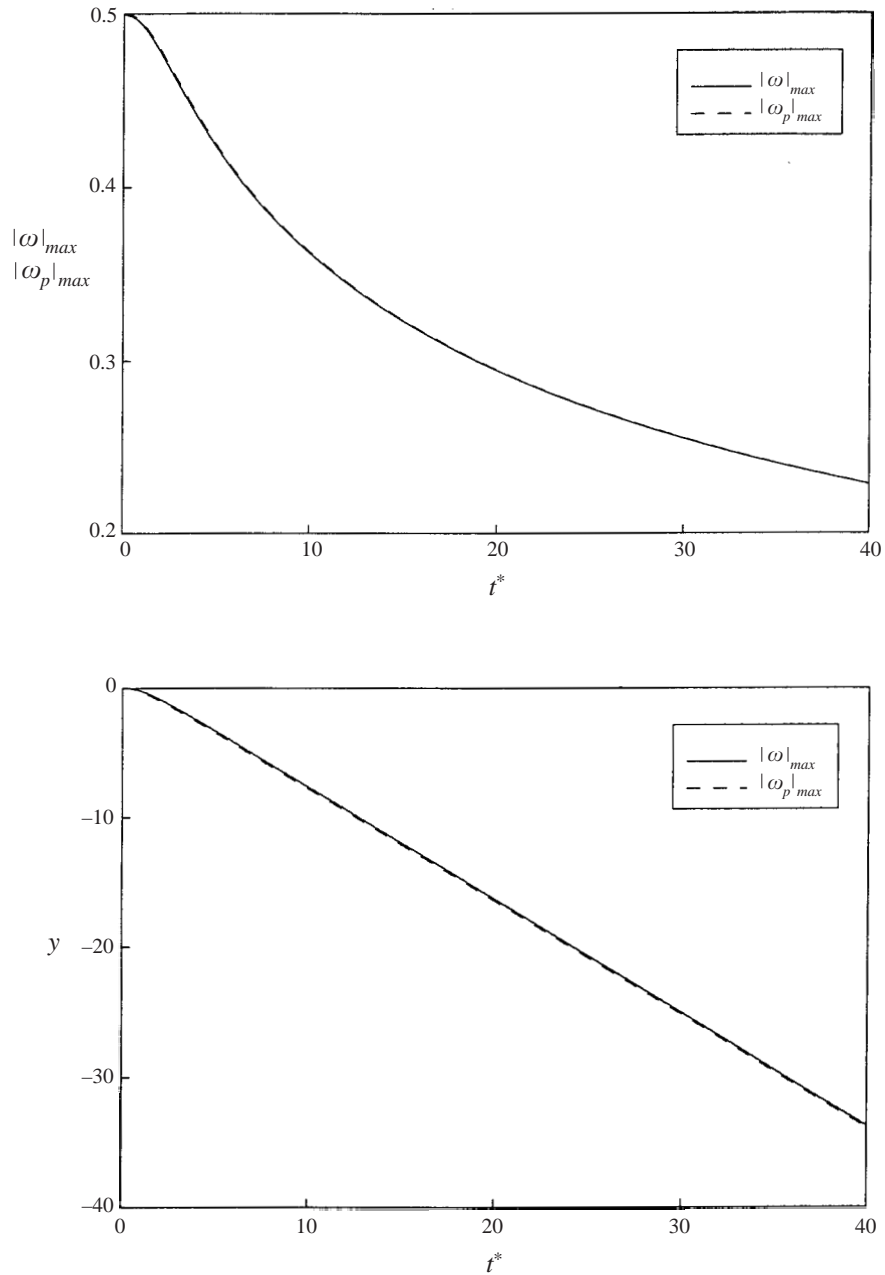FIGURE 2. Value and location of fluid and particle vorticity maxima as a function of time for $D = 0.1$, $St^2/Fr^2 = 1$, and $St/Re = 0.01$. The coupled vorticity profiles take the form of a decaying travelling wave solution.

travelling-wave-type solution, such as the one we had observed for $St^2/Fr^2 = 1$, does not develop until late in the present simulation. Interestingly, however, the evolution of the particle vorticity field leads to the transient appearance of two local maxima.

Somewhat stronger coupling is observed for $D = 1$, cf. figure 7. Even though initially the distance between the particle and fluid vorticity peaks rapidly increases,
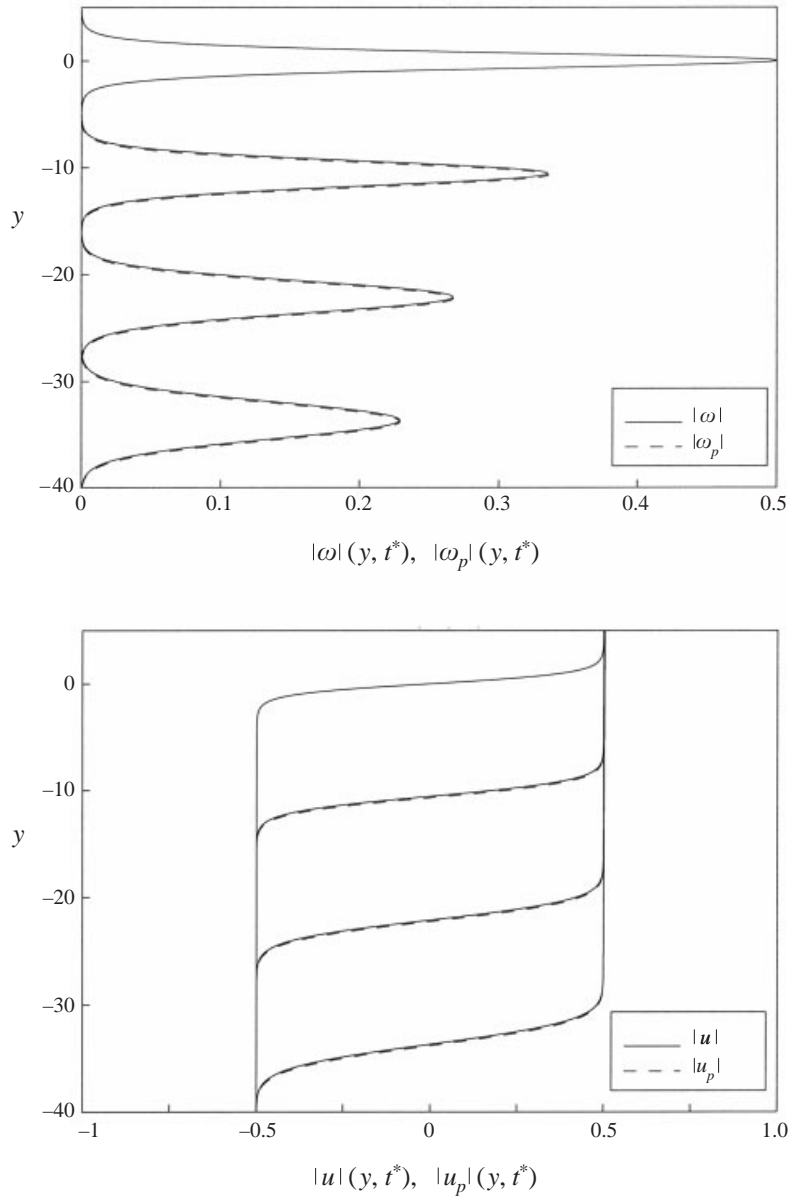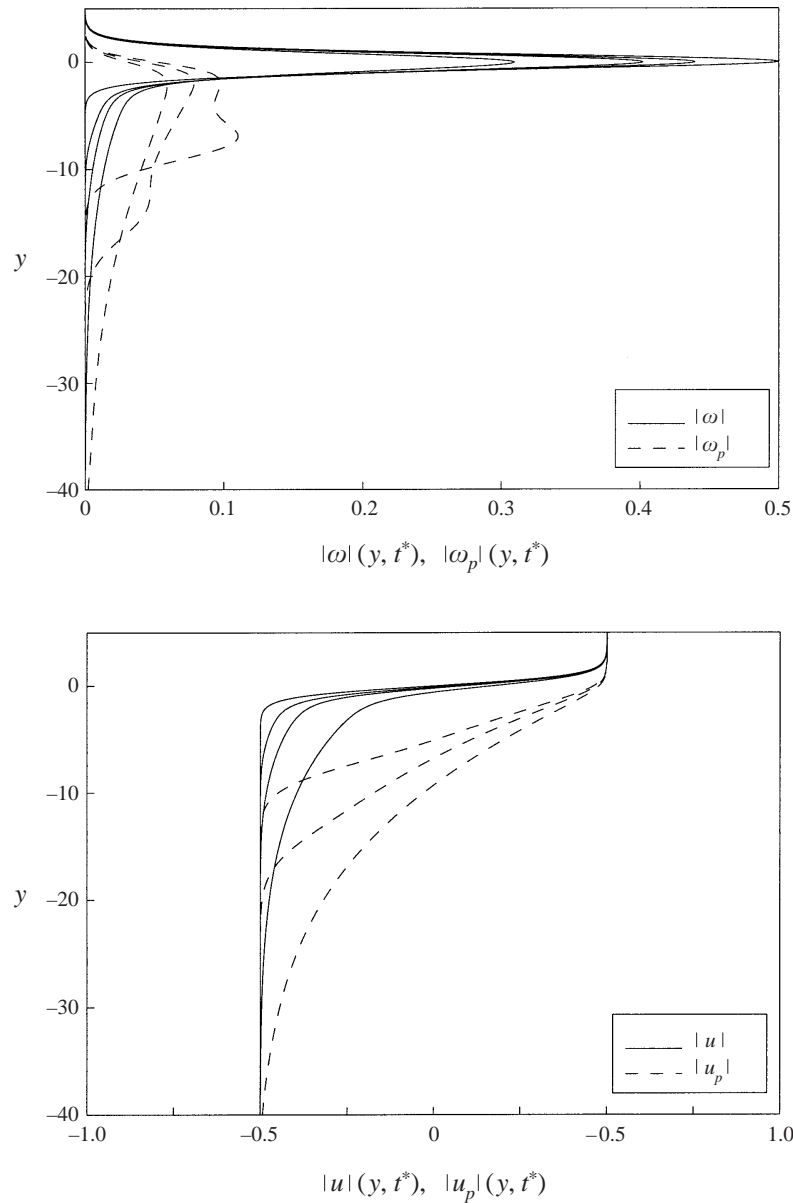
FIGURE 3. Particle and fluid vorticity and velocity profiles as function of time for $D = 10$, $St^2/Fr^2 = 1$, $St/Re = 0.01$ and times 0, 16, 32, 40. At these large mass loading parameters, the differences between fluid and particle vorticities and velocities remain small.

these peaks eventually decay and new peaks appear (cf. figure 8) that propagate downward at identical velocities. This indicates that for long times again a travelling wave solution is established. However, the initial transient behaviour with its strong non-uniformities in both the particle and the fluid vorticities, and the associated multiple inflection points in the velocity profile, may be significant as far as the stability of the flow is concerned, cf. also Chandler (1998). Finally, for $D = 10$, the behaviour once again is much more uniform, and the solution exhibits a travelling-wave-like character from the start, cf. figure 9.
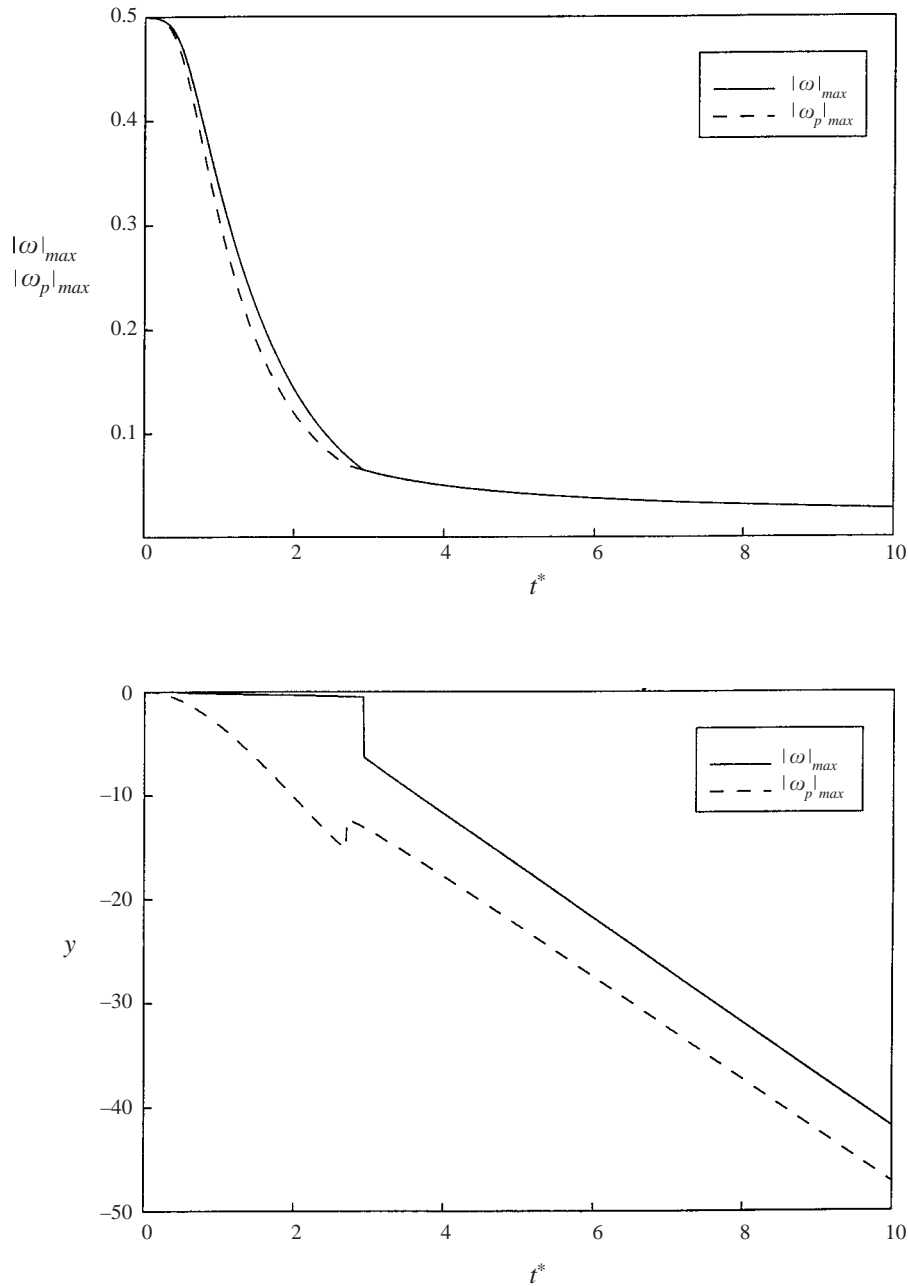
FIGURE 4. Value and location of fluid and particle vorticity maxima as a function of time for $D = 10$, $St^2/Fr^2 = 1$, and $St/Re = 0.01$. For this large value of D, fluid and particle vorticities closely track each other.

3.3.3. *Scaling argument for asymptotic propagation velocity*

The above results indicate that within certain parameter ranges, and for large times, the evolution of the fluid and particle vorticities exhibits a travelling-wave-like character. Under these circumstances, an estimate for the rate V at which the coupled vorticity peaks propagate downward can be obtained from the following momentum
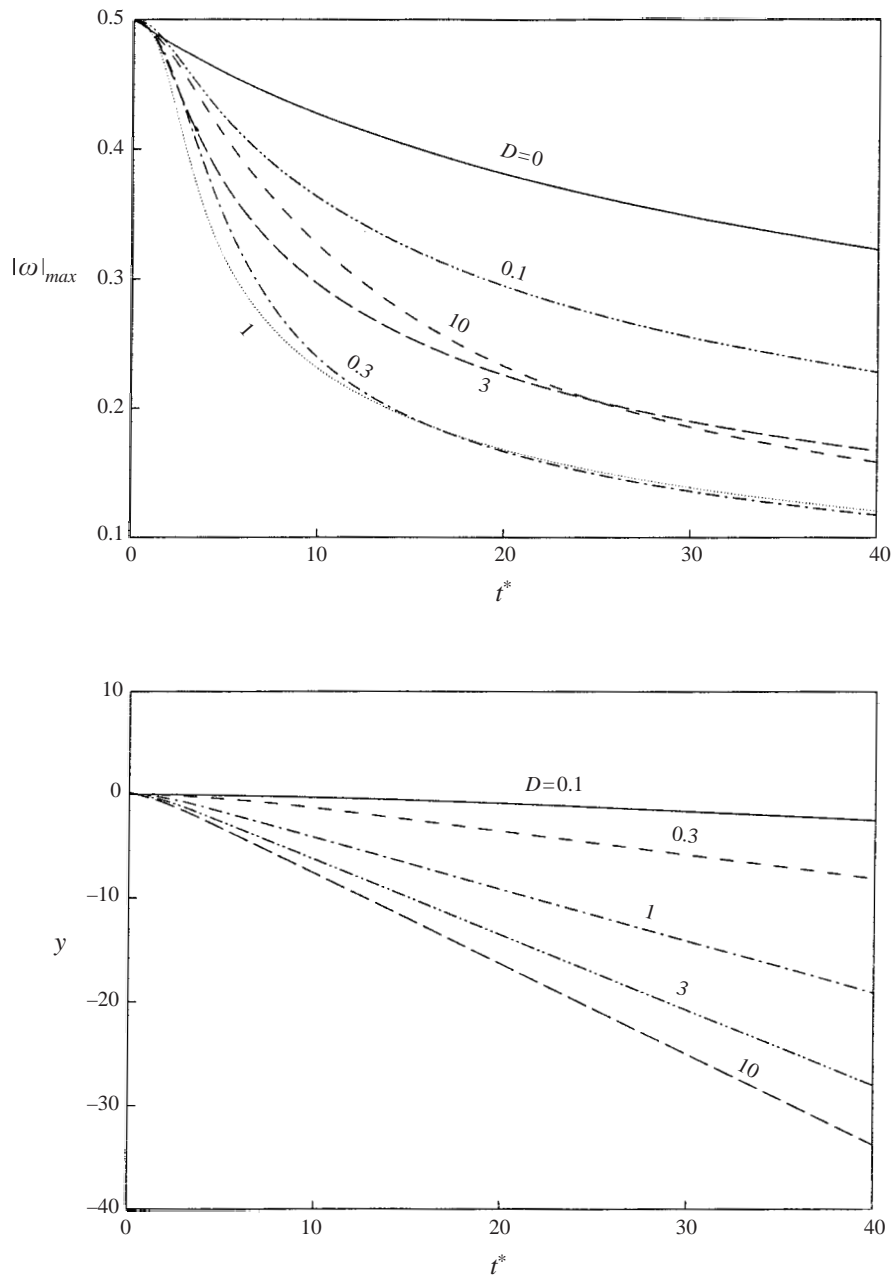
FIGURE 5. Value and location of the fluid vorticity maxima as function of time for $St^2/Fr^2 = 1$, $St/Re = 0.01$, and $D = 0.1, 0.3, 1, 3,$ and 10, respectively. The two-way coupling leads to a maximum rate of decay of the fluid vorticity for intermediate values of the mass loading parameter.

consideration. Since for $t^* \gg 1$ the particles settle with the velocity St^2/Fr^2, and since the horizontal particle and fluid velocities far above and below the mixing layer remain at 0.5 and -0.5, respectively, the particles add u-momentum to the two-way-coupled mixing layer at a rate proportional to DSt^2/Fr^2. For long times the fluid and particle profiles both propagate downward with velocity V, so that in the absence
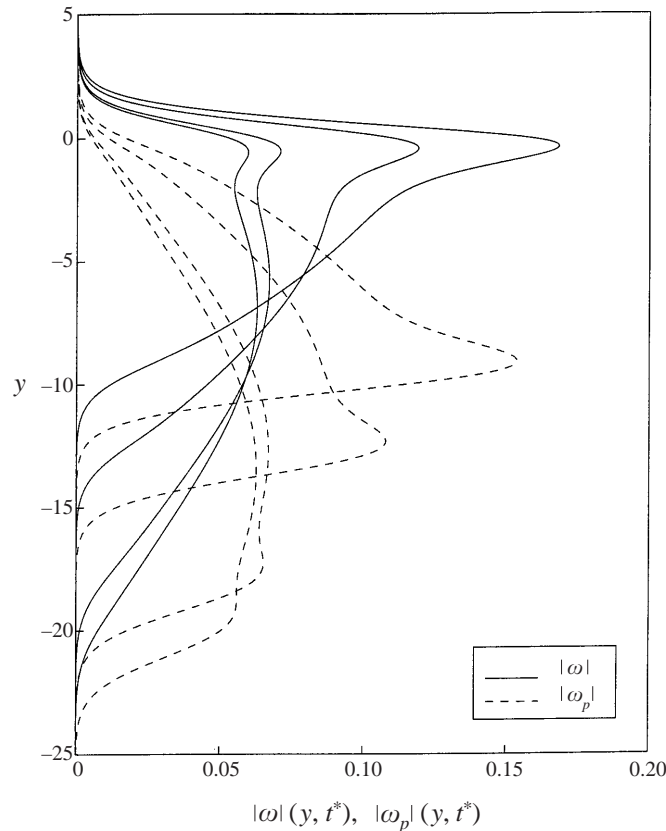
FIGURE 6. Particle and fluid vorticity and velocity profiles as function of time for $D = 0.1$, $St^2/Fr^2 = 10$, $St/Re = 0.01$ and times 0, 2, 3, and 5. At these large particle settling velocities, multiple vorticity peaks associated with multiple inflection points in the velocity profile can appear transiently.

of diffusive and/or dispersive spreading of the profiles, there is a downward flux of u-momentum at the rate of $(1 + D)V$. Balancing these two rates gives an estimate V^* for the asymptotic downward propagation velocity of the fluid and particle profiles:

$$V^* = \frac{D}{1 + D} \frac{St^2}{Fr^2}. \tag{3.25}$$

FIGURE 7. Value and location of fluid and particle vorticity maxima as a function of time for $D = 1$, $St^2/Fr^2 = 10$, and $St/Re = 0.01$. A coupled travelling wave solution emerges after an initial transient phase.

Figure 10 displays V/V^* as a function of D for a wide variety of parameter combinations, all of which were observed to eventually lead to travelling wave-type-solutions. We see that the above scaling argument provides a reasonably good estimate of the actual propagation velocity. It should be pointed out that the above scaling argument can only be expected to hold after a traveling-wave-like solution emerges.

FIGURE 8. Particle and fluid vorticity profiles as function of time for $D = 1$, $St^2/Fr^2 = 10$, $St/Re = 0.01$ and times 1.8, 2.2, 2.8 and 3.0. Again, the early stages are characterized by multiple vorticity peaks.

4. Numerical approach for the two-dimensional problem

In the following, we will focus on the temporal evolution of the above base flow (3.1) in the presence of two-dimensional, spatially periodic perturbations. Now even relatively small amounts of particle inertia will render the particle velocity field a multi-valued function of the spatial coordinates. This can easily be seen by focusing on the neighbourhood of the free stagnation point that forms midway between two evolving Kelvin–Helmholtz vortices. Locally, the directional properties of the streamline pattern in this area will cause the particulate phase to approach the stagnation point from two opposite directions, cf. the analytical and simulation results presented in Martin & Meiburg (1994). Even moderate amounts of particle inertia, i.e. values of $St \geqslant O(1)$, will then cause these particles coming from opposite directions to overshoot the stagnation point area. Consequently, in a small differential control volume element near the stagnation point, we will find particles moving in opposite directions, which shows that the particle velocity field is multi-valued. As a result, conservation equations for the particle distribution function or number density would now have to be solved in the higher-dimensional phase space, rather than in physical space. In order to avoid the associated high computational costs, we pursue a less expensive Lagrangian numerical method for the particulate phase, which is
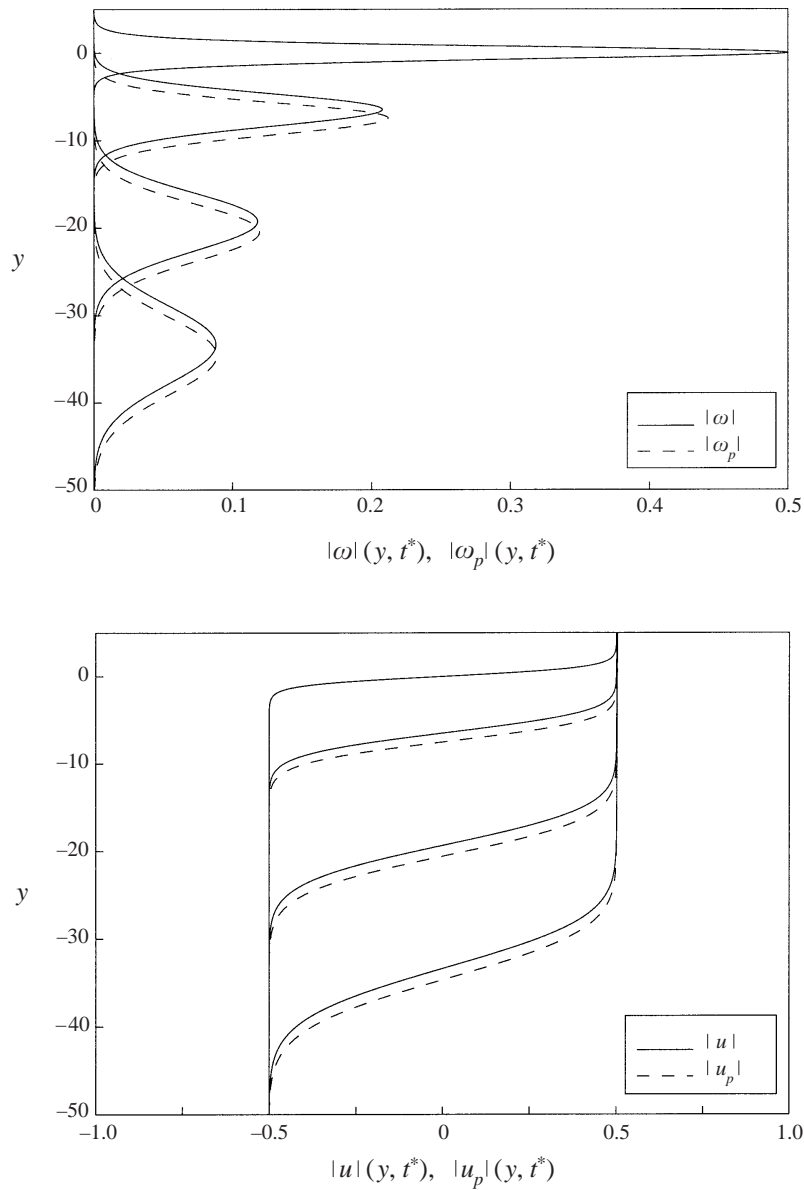
FIGURE 9. Particle and fluid vorticity and velocity profiles as function of time for $D = 10$, $St^2/Fr^2 = 10$, $St/Re = 0.01$ and times 0, 1.6, 3.2 and 5.0.

coupled to an Eulerian treatment of the fluid. Its features will be outlined in the following.

The field equations (2.17a) and (2.17b) for the fluid phase are solved in an Eulerian fashion, by applying a spectral Fourier series expansion in the streamwise, periodic direction (Gottlieb & Orszag 1977), and sixth-order compact finite differences in the transverse direction (Lele 1992). Time advancement is accomplished by means of a third-order Runge–Kutta method (Wray 1991). An initial perturbation is applied to the fluid velocity field that has the form of the eigenfunction of the most unstable mode according to inviscid theory as found by Michalke (1964). Its wavenumber
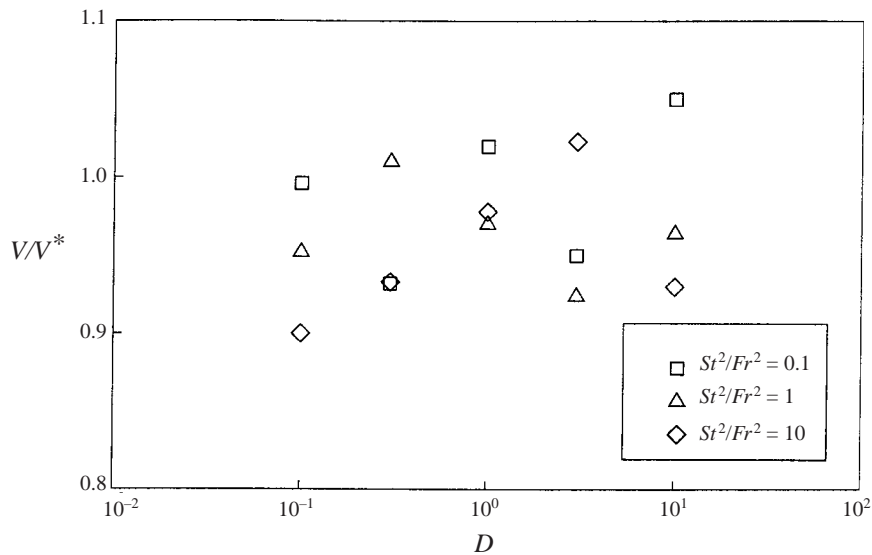
FIGURE 10. A comparison of simulation results and scaling law for the downward propagation velocity of the travelling fluid and particle vorticity waves shows reasonable agreement for the parameter range investigated here.

is $\alpha = 0.4446$, and the length of the computational domain is chosen such that it accommodates exactly one or two wavelengths, for investigations of fundamental and subharmonic perturbations, respectively. The value of Re is taken to be 200. Slip conditions are applied at the upper and lower boundaries of the control volume, which are placed sufficiently far away from the shear layer to have a negligible effect on its evolution. The simulations typically employ a discretization of 65 points per wavelength. The size of the time step strongly depends on the magnitude of the dimensionless parameters, as they effectively control the range of convection velocities and diffusive/dispersive effects. At the beginning of the simulation, the particle velocities are set equal to the local fluid velocity.

Our numerical approach for modelling the particulate phase and its effects on the fluid motion builds on the physical principles reviewed in Williams (1985), and it is similar in spirit to the techniques employed by Squires & Eaton (1990), Elghobashi & Truesdell (1993) and Maxey *et al.* (1997) in that it tracks individual particles with inertia in a Lagrangian fashion. However, while those authors focused on the two-way coupling mechanisms between the particulate phase and a turbulent carrier flow in a velocity-pressure formulation of the equations governing the fluid motion, our focus will be on gaining a vorticity-based understanding of the two-way coupling effects by which the particulate phase affects the fluid motion. Consequently, the simulations to be discussed in the following will be based on the vorticity formulation (2.17a), (2.17b) of the fluid equations of motion. Since the vorticity equation for the fluid (2.17a) involves derivatives of the particle number density field n, care has to be taken in reconstructing this field at every time level from the Lagrangian information of the individual particle locations. The numerical approach was first introduced by Wallner & Meiburg (1998) and is described in detail in the following.

The dispersed particles are tracked in a Lagrangian way, with each of the N computational particles representing a cluster of physical particles located in the

same neighbourhood. The number density field $n(x, t)$ is then obtained as

$$n(x, t) = \sum_{i=1}^{N} \Gamma_i \gamma_i [x - x_i(t)]. \tag{4.1}$$

Here γ_i represents the generic shape function of the number density distribution within computational particle i, normalized so that

$$\int \gamma_i(x) \, dx = 1. \tag{4.2}$$

In the present investigation, we take γ_i to be radially symmetric and of Gaussian shape

$$\gamma_i(r) = \frac{1}{\pi \sigma_i^2} e^{-r^2/\sigma_i^2}, \tag{4.3}$$

where σ_i is a measure of the core size of the computational cluster. Γ_i denotes the 'strength' of cluster i, i.e. the overall number of physical particles contained in it. The numerical advantage of assuming a Gaussian distribution, which is commonly done in Lagrangian numerical procedures such as vortex methods (e.g. Leonard 1980; Koumoutsakos & Leonard 1995; Meiburg 1995), is that we obtain a smooth, differentiable particle concentration field. If at time $t = 0$ the clusters are separated by a distance Δ in the x- and y-directions, we obtain

$$\Gamma_i = \Delta^2 n(x_i, 0). \tag{4.4}$$

In the numerical simulations to be discussed below, all computational clusters initially are of identical size and strength. Their initial separation Δ is typically equal to the grid size of the Eulerian mesh, while their core size $\sigma = 2\Delta$. In this way, there is sufficient overlap between the particle clusters to ensure a smooth number density field. A more formal discussion of the accuracy of this approach is currently in preparation. In order to maintain a well-resolved particle concentration field for long times, a remeshing procedure for the particles is employed which inserts an additional cluster if the distance between two initially neighbouring clusters exceeds a certain value. The strengths Γ_i of the two original clusters and the new, additional cluster are then adjusted in order to maintain the overall number of particles in the flow field. Within the present study, we follow the relatively simple rule that if the original neighbours had strengths Γ_1^* and Γ_2^* before the remeshing, their new strengths are determined as $\Gamma_1 = \frac{3}{4}\Gamma_1^*$ and $\Gamma_2 = \frac{3}{4}\Gamma_2^*$. The new cluster, which is introduced halfway between the original ones, and with their average velocity, is given the strength $\Gamma_3 = \frac{1}{4}(\Gamma_1^* + \Gamma_2^*)$.

In order to evaluate the instantaneous acceleration of each Lagrangian cluster, the flow velocity at its location is determined by means of a fourth-order, two-dimensional Lagrangian interpolation scheme (Martin & Meiburg 1994). The particle velocity is taken as a weighted average of the cluster velocities. It should be noted that this approach is valid only for a linear drag law, whereas a more complicated drag law would require a different averaging procedure. Clusters that leave the control volume in the horizontal x-direction are reintroduced at the opposite boundary, in accordance with the periodic boundary conditions in the streamwise direction. For problems in which the particulate phase is subject to gravitational forces, particle clusters are free to settle out of the computational domain through the bottom boundary. For long-time simulations, it may be necessary to continuously add new clusters at the top boundary,

in order to maintain the nominal particle number density in the upper stream. These clusters then are seeded with the horizontal fluid velocity and the instantaneous settling velocity.

An important point concerns the streamfunction boundary conditions at the top and bottom of the computational domain. For the corresponding single-phase problem, if the initial conditions and symmetry properties are such that there is no net mass flux in the horizontal x-direction, one can specify $\psi = 0$ at these boundaries for all times. For the two-way-coupled two-phase problem, on the other hand, this boundary condition will hold only if the initial conditions as well as the dynamical equations for the particulate phase satisfy corresponding symmetry properties. This will not be the case if, for example, only one of the two streams is seeded, or if gravity forces act on the particles. Under such conditions, there can be a net x-momentum transfer from the particles to the fluid, which will cause an overall acceleration of the fluid in the streamwise direction. Within our inertial reference frame, this will result in the generation of a potential component U_{pot} of the fluid velocity in the x-direction, which can be obtained as

$$\frac{\mathrm{d}U_{pot}}{\mathrm{d}t} = \frac{D}{St}\bar{s}_x, \tag{4.5}$$

where $\bar{s}_x$ denotes the x-component of the momentum source term, averaged over the entire flow field.

The numerical approach was validated by applying it to two different test problems for which the two-way-coupled equations simplify, so that in addition to the Lagrangian particle-based approach described above, they can also be solved either analytically, or numerically with standard techniques and very high accuracy for comparison purposes. Results for these two validation problems were reported in Wallner & Meiburg (1998). The first of these problems involves a fluid that is initially at rest everywhere. At $t = 0$, the entire flow field is seeded uniformly with particles of unit velocity in the x-direction. The governing equations yield for the x-velocity components of the fluid and particle velocities, respectively,

$$u(t) = \frac{D}{1+D}(1 - \mathrm{e}^{-[(1+D)/St]t}), \tag{4.6a}$$

$$u_p(t) = \frac{1}{1+D}(D + \mathrm{e}^{-[(1+D)/St]t}). \tag{4.6b}$$

A variant of Stokes' first problem serves as a second, more challenging test case. An infinite flat plate is impulsively accelerated from rest to a constant velocity in its own plane. Liu (1966) formulates the equations governing the temporal evolution of the fluid and particle phases above the plate. In our notation, they are

$$\frac{\partial u}{\partial t} = \frac{1}{Re}\frac{\partial^2 u}{\partial y^2} + \frac{D}{St}(u_p - u), \tag{4.7a}$$

$$\frac{\partial u_p}{\partial t} = \frac{1}{St}(u - u_p). \tag{4.7b}$$

For both of these test problems, the numerical approach described above was able to provide very accurate solutions, cf. Wallner & Meiburg (1998).
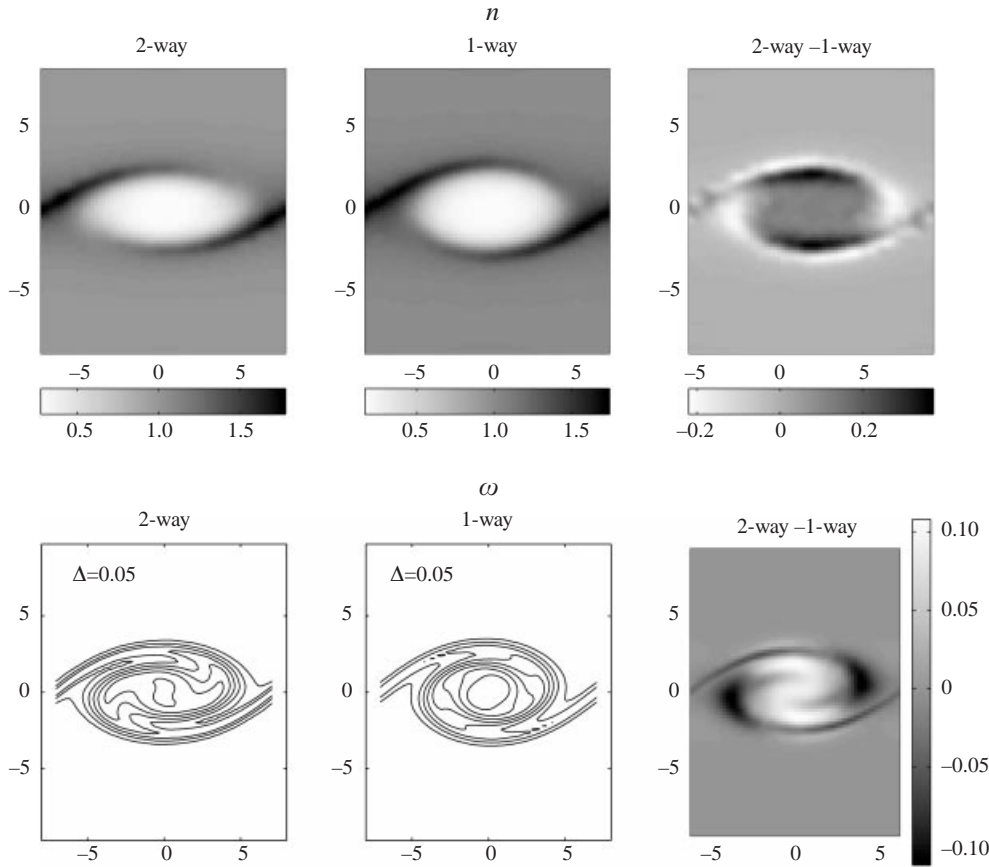
FIGURE 11. $St = 1$, $D = 0.5$, $Re = 200$: concentration and vorticity fields for the two-way-coupled and the one-way-coupled (passive) case, respectively, at time $t = 37.5$. The right-hand column shows the differences between the two flows. In the vorticity contour plots, Δ gives increments between contour levels. The vorticity difference is indicated by shading, with dark (light) shading visualizing an increase (decrease) in the vorticity magnitude due to coupling. The particle number density is seen to increase in the core, while the vorticity decreases.

5. Results of two-dimensional simulations

5.1. *Interplay of particle inertia and vorticity dynamics*

5.1.1. *Uniform particle loading*

In the following, some of the qualitative differences in the vorticity and concentration fields between the one-way coupled and the two-way coupled cases will be described, at first in the absence of gravitational settling effects. To this end, we will focus on the case of $St = 1$, for which the coupling between the two phases is quite pronounced, as will be seen below. For an initially uniform seeding with particles, and for a mass loading of $D = 0.5$, significant differences in the evolution of the mixing layer at $Re = 200$ are visible, cf. figure 11. Both in the braids, as well as in the regions to the immediate left and right of the core, an increase in the magnitude of the vorticity due to the two-way coupling can be observed. In contrast, the vorticity within the core, and in the regions immediately above and below it, is reduced in magnitude. Based on the results obtained by Druzhinin (1995b) for the model flow of a Stuart vortex, and the linear stability analysis by Dimas & Kiger (1998), this behaviour is
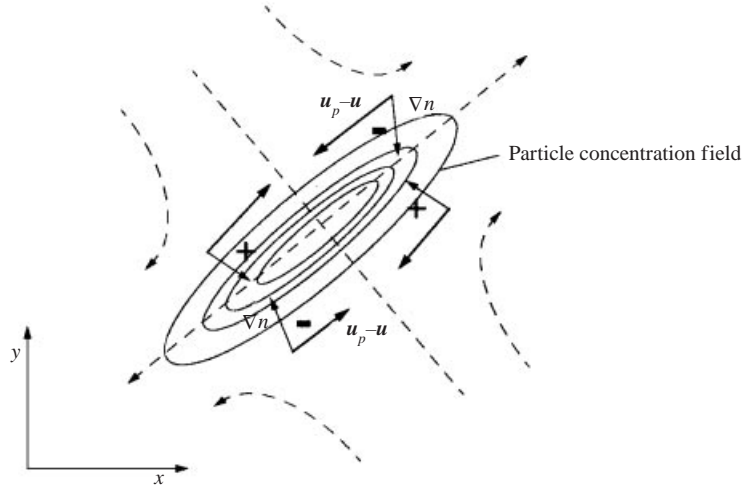
FIGURE 12. Principal mechanism of vorticity generation in the braid region for a uniformly seeded flow, due to the misalignment of the particle concentration gradient and the slip velocity. The isocontours indicate the band of high particle concentration aligned with the extensional direction of the stagnation point flow field. Maximum particle concentrations are reached near the stagnation point. The gradient vector ∇n thus points towards the streamline emanating from the stagnation point. Due to their inertia, the particles do not accelerate away from the stagnation point as quickly as the fluid, so that the slip velocity $u_p - u$ points against the direction of the streamline leaving the stagnation point. The cross-product of these two vectors results in regions of vorticity production and cancellation, as indicated by '−' and '+', respectively.

in line with expectations. Furthermore, we observe that the braids remain somewhat thicker under two-way coupling, and that the vortex generally is less circular than in the passive case.

The particle concentration field is affected by the two-way coupling as well. As the coupling reduces the core vorticity, the centrifugal forces acting on the particles become weaker. As a result, for two-way coupling we observe a slight increase in particle concentration in the core, with a corresponding decrease in the braids. Due to the less pronounced ejection of particles from the core, the concentration field appears somewhat compressed in the cross-stream direction, when compared to the passive case. This behaviour is again consistent with the predictions by the linear stability analysis of Dimas & Kiger (1998).

A more detailed understanding of the underlying vorticity production and destruction mechanisms due to particle loading can be obtained by analysing the source term in the fluid vorticity equation (2.17*a*). Upon expanding

$$\nabla \times [n(\bar{u}_p - u)] = \nabla n \times (\bar{u}_p - u) + n(\nabla \times \bar{u}_p - \nabla \times u), \qquad (5.1)$$

two potential mechanisms for vorticity generation/loss are identified. The first term indicates that the vorticity will be altered if the concentration gradient is misaligned with the direction of the slip velocity. The second term describes the influence of a difference between the particle and fluid vorticities. The simulations usually show that in the vicinity of the core, the second term is largest, due to the particles' inertia. Keeping in mind that the fluid vorticity is negative everywhere, the source term will thus be positive in the core, thereby reducing the fluid vorticity. In the braids, on the other hand, the first term on the right-hand side of equation (5.1) becomes more significant due to the large variations of the particle concentration field, and the
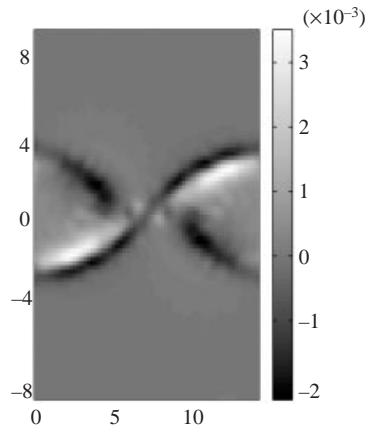
FIGURE 13. The source term in the fluid vorticity equation for a uniformly seeded flow with $St = 1$, $Re = 200$, $D = 0.1$, and $t = 25$. Dark (light) shading indicates areas of vorticity production (cancellation). The postulated quadrupole structure of the source term in the braid region can clearly be recognized.

relatively weak vorticity. In combination with the local slip velocities, it leads to both production and destruction of vorticity in the braid region, as shown in the sketch of figure 12. As both fluid and particles are being accelerated away from the stagnation point, the slip velocity $u_p − u$ points towards the stagnation area, due to the particle inertia. When combined with the local direction of the particle number density gradient, this feature suggests a quadrupole structure of the vorticity source term near the stagnation point, which is confirmed by the numerical result shown in figure 13.

Overall, the vorticity generation and destruction caused by the two-way coupling is seen to slow the transport of vorticity from the braids into the core region, thereby weakening the Kelvin–Helmholtz instability mechanism of the fluid phase. In this context, it should be pointed out that the two-way coupling effectively results only in the redistribution, but not in any net generation, of fluid vorticity. This can easily be seen from the fact that the flow field remains periodic in the streamwise direction, and that far above and below the mixing layer the horizontal fluid velocity maintains its original value. Consequently, the circulation per wavelength of the mixing layer is not affected by the two-way coupling. The above numerical findings for the nonlinear stages of the mixing layer evolution again are in agreement with the inviscid linear stability analysis of a particle-laden mixing layer conducted by Dimas & Kiger (1998). These authors find the two-way coupling to have the effect of removing vorticity from the core and adding it to the braids. Furthermore, some similarities can be found with observations made by Ruetsch & Meiburg (1994) on two-way coupled mixing layers with bubbles. Bubbles are seen to have a similar effect in that they reduce the vorticity in the vortex core.

For a comparatively high Stokes number of 10, a slightly different behaviour is observed, cf. figure 14. Similarly to the case of intermediate Stokes number, a decrease in the magnitude of core vorticity is observed. However, these heavier, less responsive particles form streaks with a smaller angle of inclination in the braids. Furthermore, now *two* bands of high particle concentration are found in the braid region, in agreement with the one-way-coupled analysis presented by Martin & Meiburg (1994). This behaviour represents a classic example of the multi-valued particle velocity fields
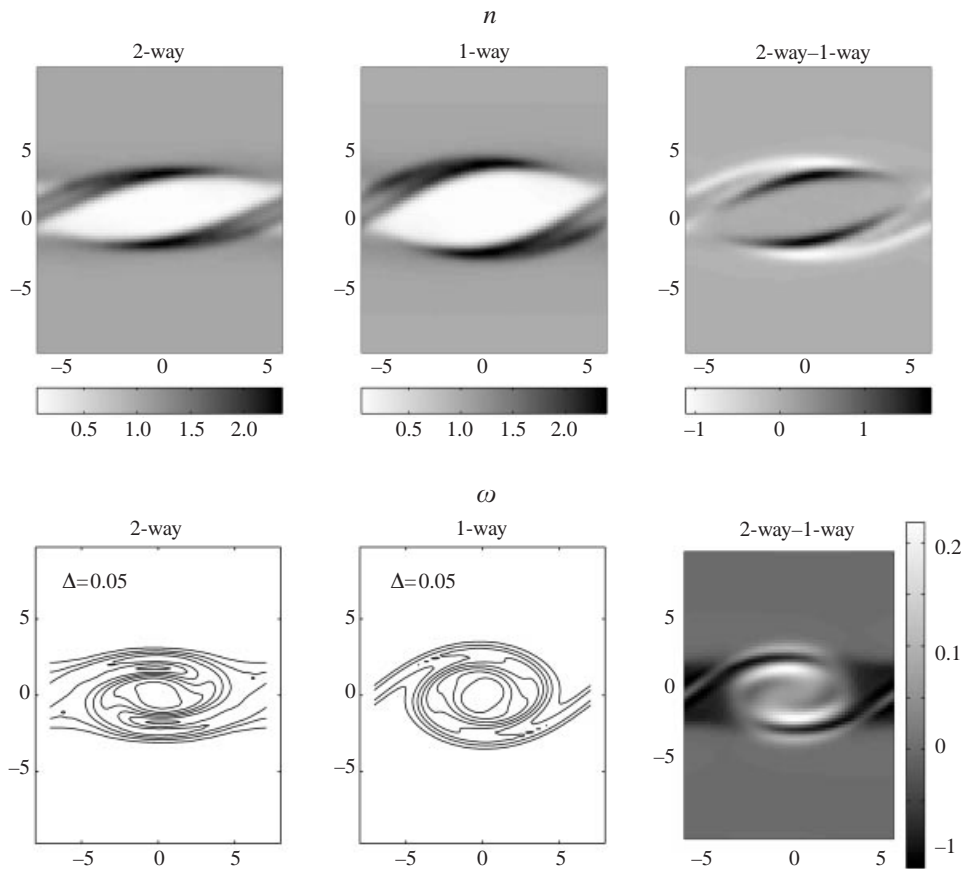
n

ω

FIGURE 14. $St = 10$, $D = 0.5$, $Re = 200$: concentration and vorticity fields for the two-way-coupled and the one-way-coupled (passive) case, respectively, at time $t = 37.5$. The right column shows the differences between the two flows. The braids are thickened by the two-way coupling effects, while the particle concentration field is compressed in the cross-stream direction. Note the existence of two bands of high particle concentrations in the braid region, in agreement with the analysis of Martin & Meiburg (1994).

that exist for even moderately large values of St. Clouds of underdamped particles approach the stagnation point from opposite directions and overshoot it, so that particles with opposite velocities coexist near the stagnation point. As they are forced back by the oncoming flow on the other side of the stagnation point, they form high-concentration bands. Consequently, the existence of *two* such bands could not be captured with numerical simulations based on governing equations that assume single-valued particle velocity fields.

In the following, the effect of St and D on the nonlinear stages of the mixing layer growth will be quantified. To this end, we analyse the temporal growth of the maximum of the streamfunction perturbation for different values of St and D, cf. figures 15, 16 and 17. As expected on the basis of the above discussion, for intermediate and high St values the damping effected by the particulate phase increases uniformly with the mass loading, since the source term in the vorticity transport equation is proportional to D. This agrees with the linear stability predictions of Dimas & Kiger (1998), as well as with Yang *et al.* (1990). For comparable mass loadings, the damping is more pronounced at larger St values.
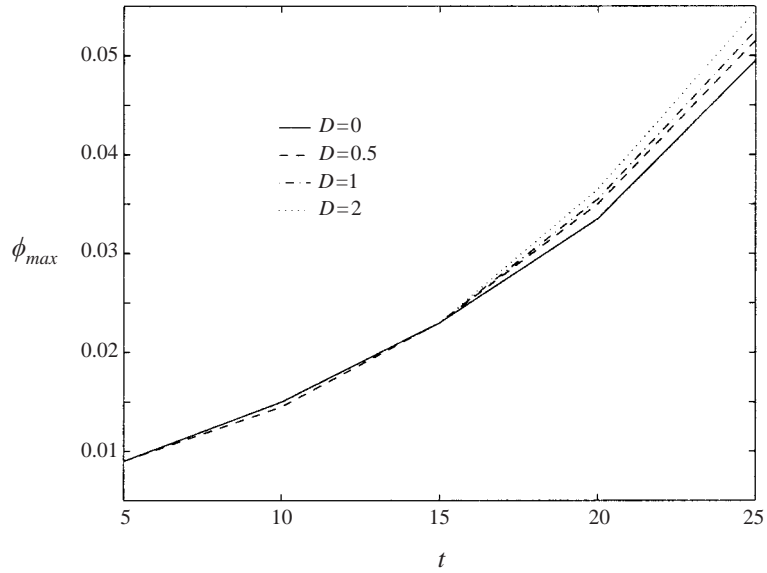
FIGURE 15. Maximum of the streamfunction perturbation as a function of time for $St = 0.1$ and $Re = 200$ with uniform particle loading. Increased loading slightly destabilizes the mixing layer.
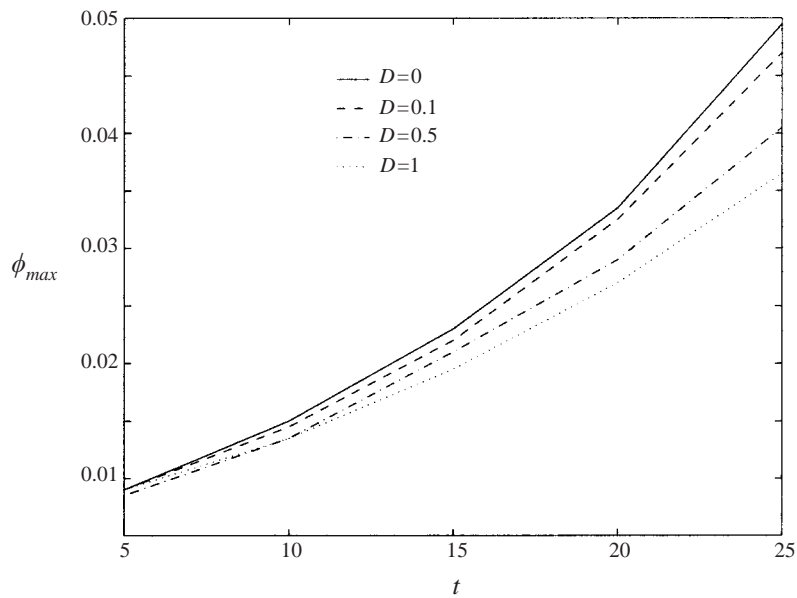

FIGURE 16. As figure 15 but for $St = 1$. Increased loading leads to a more pronounced damping of the mixing layer perturbation.

For $St \ll 1$, increased mass loadings are observed to slightly destabilize the mixing layer, figure 15. Based on arguments put forward earlier by Saffman (1961), this behaviour is not unexpected. Saffman reasons that a loading of fine particles with a $St \ll 1$ should be destabilizing, as these particles tend to move with the fluid, so that their main effect is to increase the effective density of the gas, and thereby the effective Reynolds number. In contrast, for $St \gg 1$, he demonstrates that the term due
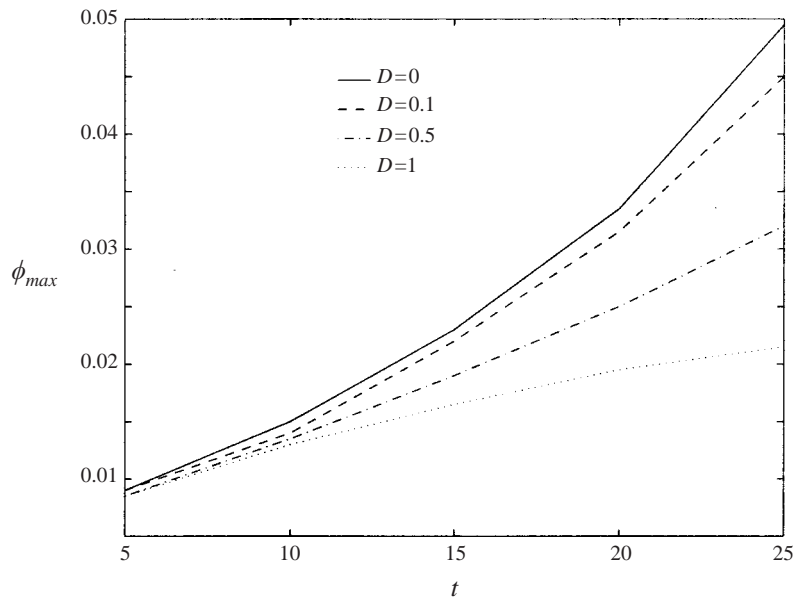
FIGURE 17. As figure 15 but for $St = 10$. The damping is seen to be even more pronounced than for $St = 1$.

to coupling appears as an additional frictional force in the fluid momentum equation, which dissipates kinetic energy and thereby stabilizes the flow. We remark that the linear stability analysis by Dimas & Kiger (1998) addresses inviscid dynamics, so that an effective increase in the Reynolds number cannot be captured. For all of the above considerations, it should be noted that we are comparing the growth of perturbations of equal wavenumbers, rather than the wavenumbers of maximum amplification, which can change with particle loading. However, Yang *et al.* (1990) show that this wavenumber depends only weakly on D.

It is also instructive to evaluate the influence of St on the flow for constant values of D, cf. figure 18. For $St \ll 1$, there is a slight amplification compared to the single-phase flow. With growing St, the particulate phase increasingly dampens the Kelvin–Helmholtz instability. Then, as a critical range of $St \approx 5 - 8$ is exceeded, the damping weakens again. This confirms our earlier suspicion that the influence of St cannot be predicted as easily as that of D, since the St value influences both the particle response as well as the source term in the vorticity equation. Since an increase in St for a given value of D corresponds to reducing the number of particles while increasing their size, the implication is that the competition between the effects of particle number and size, respectively, depends on St.

5.1.2. *Differential particle loading*

Here the focus will be on the case where only one of the streams that make up the mixing layer is seeded with particles. Again, the initial particle velocity is equal to the fluid velocity at the particle location. Now, the flow field contains a region of strong particle number density gradients from the beginning, so that we expect to see an effect of the particulate phase on the fluid vorticity from the start. This is in contrast to the uniformly seeded flow without gravity analyzed above, where such gradients only evolved with time as particles accumulated in some regions, while being ejected from others.
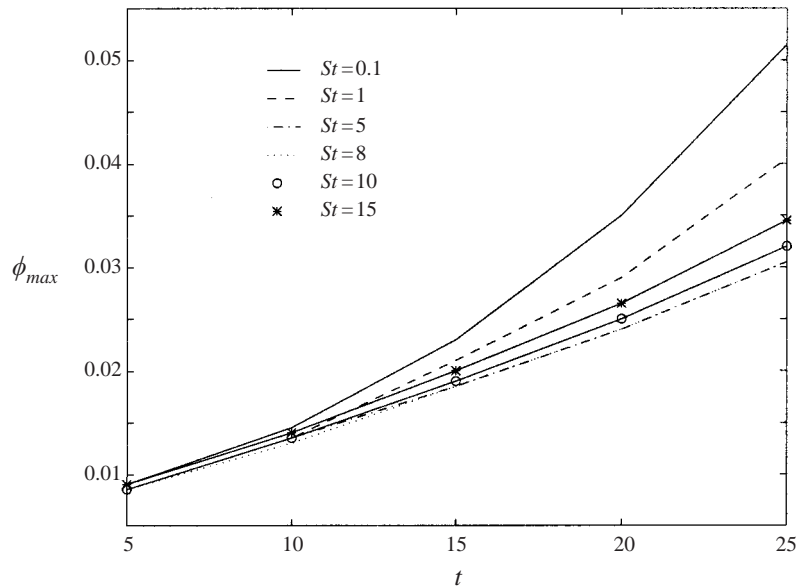
FIGURE 18. Maximum of the streamfunction perturbation as a function of time for $D = 0.5$, $Re = 200$ and various St values. Up to $St \approx 5$–8, the damping effect increases with St. For even larger St, the damping effect is reduced again. Note that the curves for $St = 5$ and $St = 8$ are almost on top of each other.

The principal effects of two-way coupling on the vorticity and particle concentrations for differential loading can be seen in figure 19, which shows the case of $St = 1$, $D = 0.5$, and $Re = 200$ at time $t = 37.5$. The symmetry properties of the uniformly seeded flow are no longer preserved, and instead the spatial distribution of the vorticity source term results in a net shift of the Kelvin–Helmholtz vortex in the direction of the seeded stream. The net momentum transferred to the fluid by the particulate phase can thus be seen to render the Kelvin–Helmholtz instability dispersive. This agrees with the linear stability findings of Wen & Evans (1994) for an inviscid mixing layer. It should be emphasized that the net motion of the concentrated vorticity region is not so much a convection effect as it is caused by the spatial gradients in the production and destruction of vorticity. In the braid region, the quadrupole nature of the vorticity source term observed for uniform particle loading is replaced by a dipole distribution for the case of differential particle loading, cf. the sketch in figure 20 and the simulation result in figure 21. This results in a strengthening of the upstream half of the braid, which is located in the initially unseeded stream, while the downstream half, located in the seeded stream, is depleted of vorticity, so that the vortex core appears to be 'cut off' from its braid.

For uniformly seeded mixing layers, two-way coupling effects had been fairly weak if $St \ll 1$. This is no longer the case if only one of the streams is seeded, cf. figure 22. The strong local gradients in the particle number density field result in the generation of a considerable amount of vorticity, even for small slip velocities. Consequently, the vorticity magnitude can be seen to increase substantially in parts of the vortex core. For larger St values, on the other hand, the situation is somewhat different, cf. figure 23. Due to the slower response of the particles, the interface does not roll up as much as for lower Stokes numbers. As a result, a thickening of the braid region is observed, rather than the 'cut off' seen for smaller St.
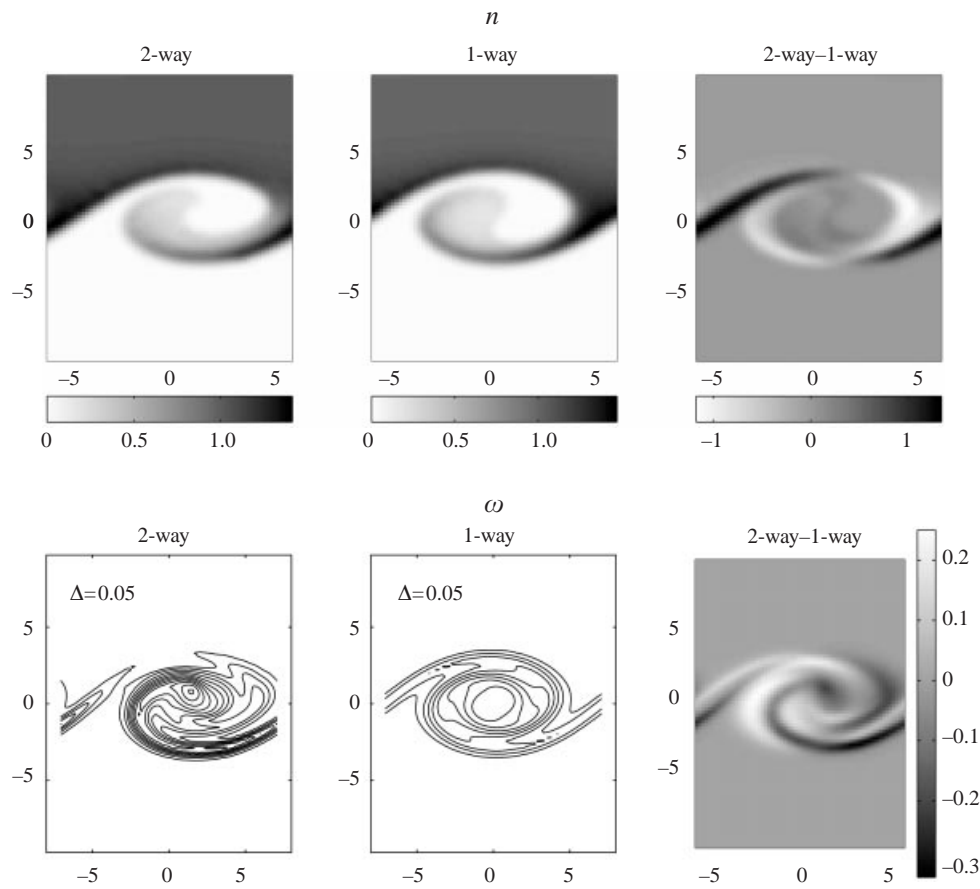
FIGURE 19. $St = 1$, $D = 0.5$, $Re = 200$: initially, only the upper stream is seeded with particles. Shown are the concentration and vorticity fields for the two-way-coupled and the one-way-coupled (passive) case, respectively, at time $t = 37.5$. The right-hand column shows the differences between the two flows. The asymmetric nature of the vorticity source term distribution leads to a net displacement of the Kelvin–Helmholtz vortex in the direction of the seeded stream. While the vorticity intensifies in the braid segment located in the unseeded stream, it is approximately cancelled where the braid reaches into the seeded stream.

Some similarities can be observed between the present case of a differentially loaded mixing layer and that of a density-stratified shear layer, cf. the investigation by Lawrence *et al.* (1991). For stably stratified shear layers at small Richardson numbers, these authors experimentally observe structures similar to Kelvin–Helmholtz billows in the homogeneous case, except for a stronger asymmetry of the flow. This resembles our findings for $St = 0.1$, which indicates that the particle loading in the present problem can play a role similar to that of the stratification in single-phase flows. The above authors also conduct a linear stability analysis of the inviscid, stratified shear layer. If the inflection points of the velocity and density profiles, respectively, are displaced from each other, they observe the occurrence of two unstable modes travelling in opposite directions. This finding is again relevant to the present particle-laden flow, as gravitational settling can lead to an offset between the inflection points in the velocity and concentration profiles.

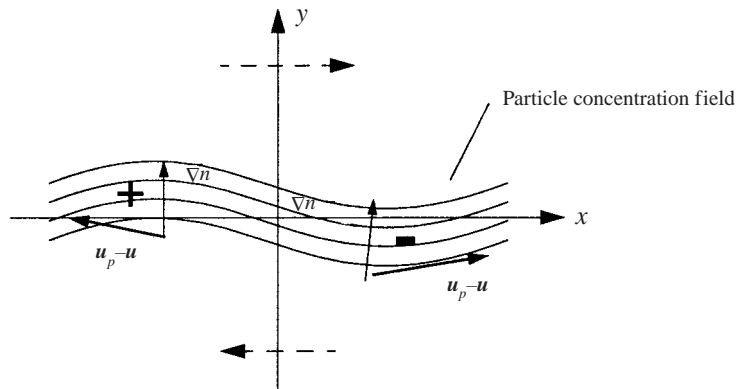Further details regarding the above flows, along with additional quantitative infor-

FIGURE 20. Principal mechanism of vorticity generation in the braid region for a differentially seeded flow, due to the interaction between the particle concentration gradient and the slip velocity. Regions of vorticity production and cancellation are indicated by '−' and '+', respectively.
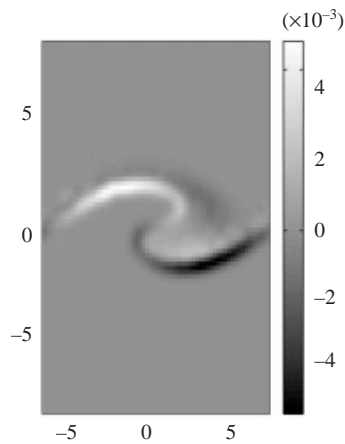

FIGURE 21. The source term in the fluid vorticity equation for a differentially seeded flow with $St = 1$, $Re = 200$, $D = 0.1$, and $t = 25$. Dark (light) shading indicates areas of vorticity production (cancellation). In contrast to the uniformly seeded flow, the source term now has a dipole structure in the braid region.

mation on such global diagnostic measures as the displacement thickness (Martin & Meiburg 1994), can be found in Wallner (1998).

5.1.3. *Subharmonic perturbations and vortex pairing*

Winant & Browand (1974) observed vortex pairing to be the dominant mechanism responsible for the growth of mixing layers. In the present simulations, such a vortex pairing event was triggered by adding to the initial basic perturbation a subharmonic one of equal amplitude and appropriate phase. Keeping in mind the above results for fundamental perturbations, as well as the one-way-coupled vortex pairing results of Martin & Meiburg (1994) and the experimental observations of Kiger & Lasheras (1995), figure 24 does not reveal any major surprises regarding the two-way-coupled evolution of vortex pairing events. Damping of the fundamental perturbation leads to decreasing vorticity magnitudes in the cores of the pairing vortices, while the vorticity
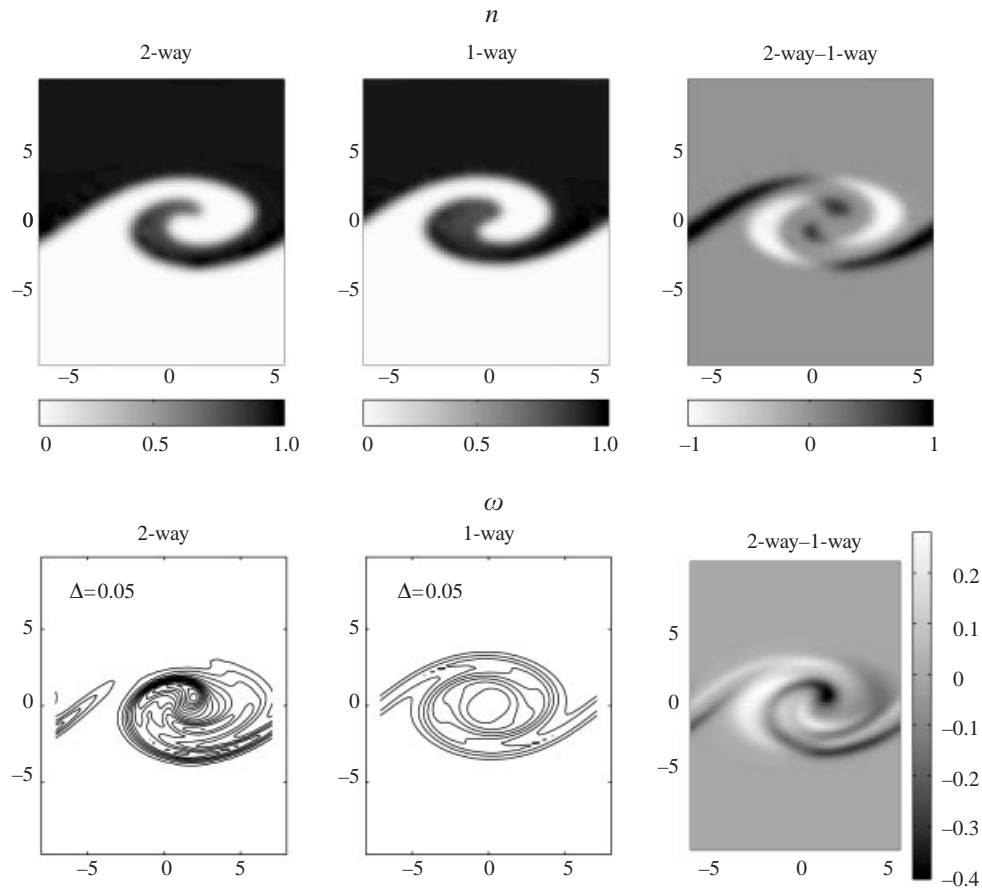
n

ω

FIGURE 22. $St = 0.1$, $D = 0.5$, $Re = 200$: concentration and vorticity fields for the differentially seeded flow. Shown are the two-way-coupled and the one-way-coupled (passive) case, respectively, at time $t = 37.5$. The right-hand column shows the differences between the two flows. In contrast to uniformly seeded flows, two-way coupling effects are strong even for small values of St.

in the braids shows a slight increase. The strong strain in between pairing vortices rapidly depletes this area of particles, while the braid connecting pairs of vortices maintains a high particle concentration. Overall, the nature of the pairing mechanism does not seem to be strongly affected by the particulate phase for the present parameter combination. A similar conclusion holds for the case of a differentially loaded, subharmonically growing mixing layer. More detailed information on this case is provided by Wallner (1998).

5.2. *Gravitational settling and vorticity dynamics*

Inspection of equation (2.17a) shows that gravity does not directly enter the conservation equation for the vorticity. Rather, there are two ways in which gravitational forces affect the vorticity production term indirectly. First, by causing the particles to settle through the fluid, gravity tends to convectively modify the gradient field of the particle number density, thereby altering the locations of vorticity production and cancellation. Secondly, the gravitational acceleration of the particles affects their slip
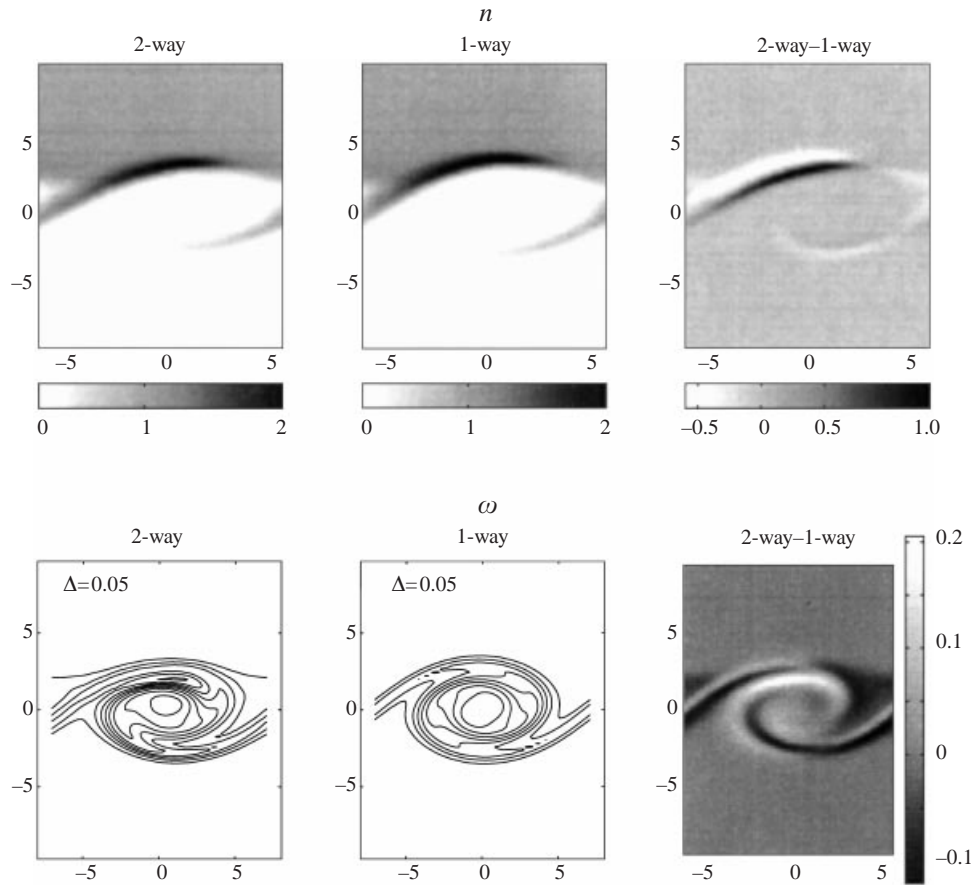
FIGURE 23. $St = 10$, $D = 0.5$, $Re = 200$: concentration and vorticity fields for the differentially seeded flow at time $t = 37.5$. At these larger St values, the braid is thickened by the two-way coupling effects rather than 'cut off', as was the case for smaller St.

velocity, which again affects the vorticity source term. Here these two mechanisms will be briefly discussed for uniformly seeded particle-laden mixing layers.

The case of $St = Fr = 3$, $D = 0.1$, and $Re = 200$ is well suited for demonstrating the qualitative changes caused by the two-way coupling. Figure 25 shows that two-way coupling results in a global shift of the vorticity field in both the $+x$- and the $-y$-directions. This is effected by the vorticity source term, which tends to cancel the vorticity on the upper side of the mixing layer, while amplifying it on the lower side, cf. figure 26. A similar trend is seen in the corresponding particle concentration field, cf. figure 27. This downward shift of the vorticity by means of production and cancellation on alternating sides is similar in principle to our findings for the unidirectional base flow in §3.

In order to find the effective velocity at which the above horizontal and vertical shifts occur, we evaluate the distance by which the two-way coupled vorticity field would have to be displaced in the x- and y-directions in order to be optimally correlated with the one-way coupled field. This approach is similar in spirit to the well-established experimental technique of digital particle image velocimetry (DPIV, e.g. Fincham & Spedding 1997). In this way, we obtain data sets such as the ones
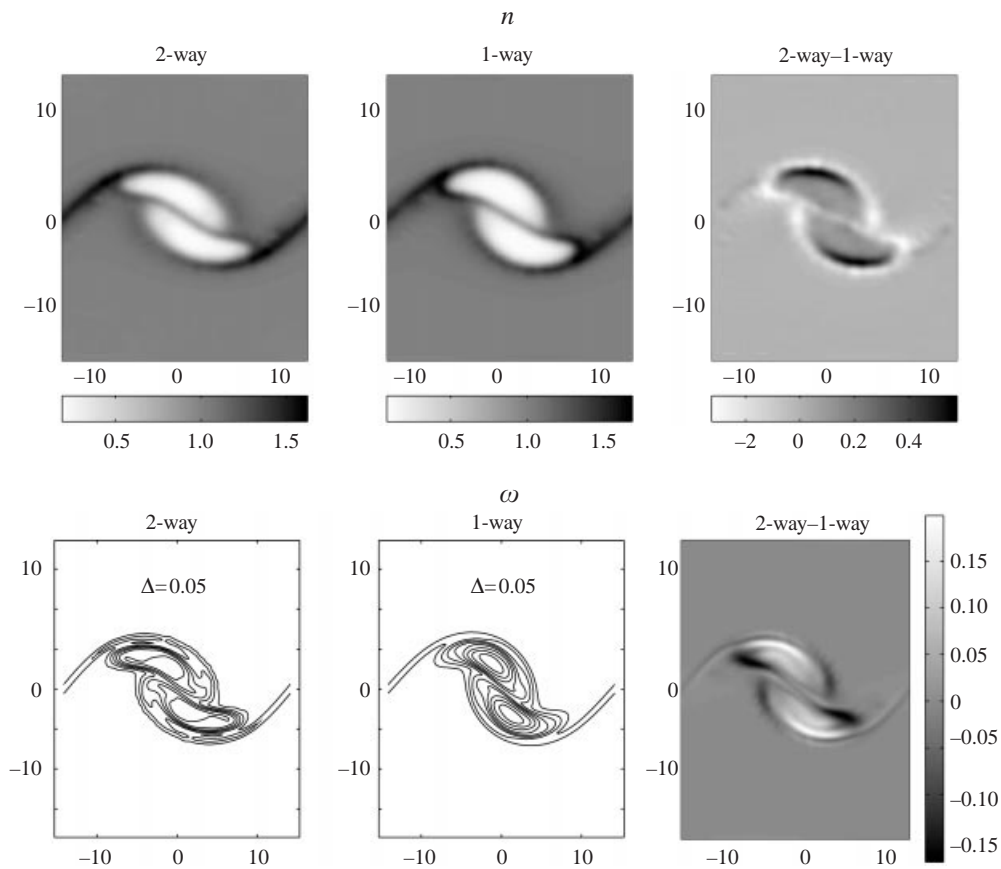
FIGURE 24. $St = 1$, $D = 0.5$, $Re = 200$: uniformly seeded flow with vortex pairing at time $t = 50$. Shown are the concentration and vorticity fields for the two-way-coupled and the one-way-coupled (passive) case, respectively. The damping caused by the particulate phase leads to a certain slowdown of the vortex pairing process, without significantly modifying its fundamental dynamics.

shown in figure 28, where the length of the error bars indicates the resolution of the computational grid. These figures, as well as many others for different parameter combinations, suggest that after an initial transient the vortical structure assumes nearly constant velocities in the horizontal and vertical directions, which can be estimated from least-squares fits of the displacement data.

Our investigation of the two-way coupled, unidirectional base flow in §3 suggested that over a wide range of parameters the long-time asymptotic effective downward propagation velocity of the fluid and particle velocity profiles scale with $D/(1 + D)(St^2/Fr^2)$. Figure 29 compares the two-dimensional simulation results with this scaling law. It is seen that for the present, limited parameter range the agreement is quite good.

6. Summary and conclusions

The present investigation aims at developing a vorticity-based understanding of the two-way coupling effects in dilute particle- or droplet-laden mixing layers, with and without particle settling. Some fundamental insight is gained by analysing a
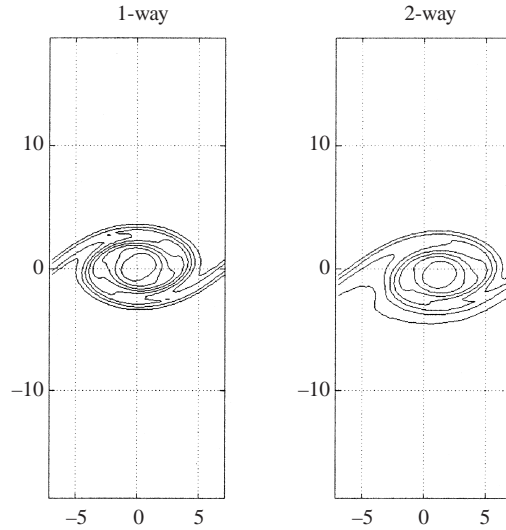
FIGURE 25. $St = 3$, $Fr = 3$, $D = 0.1$, $Re = 200$: uniformly seeded flow at time $t = 37.5$. Shown are the respective vorticity fields for one-way and two-way coupling. The two-way coupling results in a net horizontal displacement of the large scale vortical structure in the direction of the upper stream. At the same time, it is shifted downward in the direction of the gravitational acceleration.
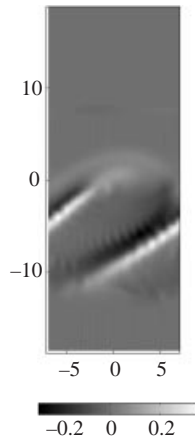

FIGURE 26. The source term in the fluid vorticity equation for the uniformly seeded flow of figure 25. Light (dark) shading indicates areas of vorticity production (cancellation).

unidirectional mixing layer type base flow. For this model flow, a set of conditions can be established that renders the particle velocity field a single-valued function of space for all times. Under these conditions, a simplified set of two-way-coupled equations governing the vorticity of the fluid and particulate phases, respectively, is derived. The two-way coupling shows up in the form of source terms in these two vorticity equations. Numerical solutions of these equations demonstrate the formation of a decaying travelling wave solution over a wide range of parameters. Interestingly, the downward propagation of the fluid vorticity field is not accomplished through convection, but rather by the production and loss of vorticity on opposite sides of the mixing layer. The particle vorticity field evolves through the interaction of convection effects, caused by the settling motion, with the production and loss of vorticity. The
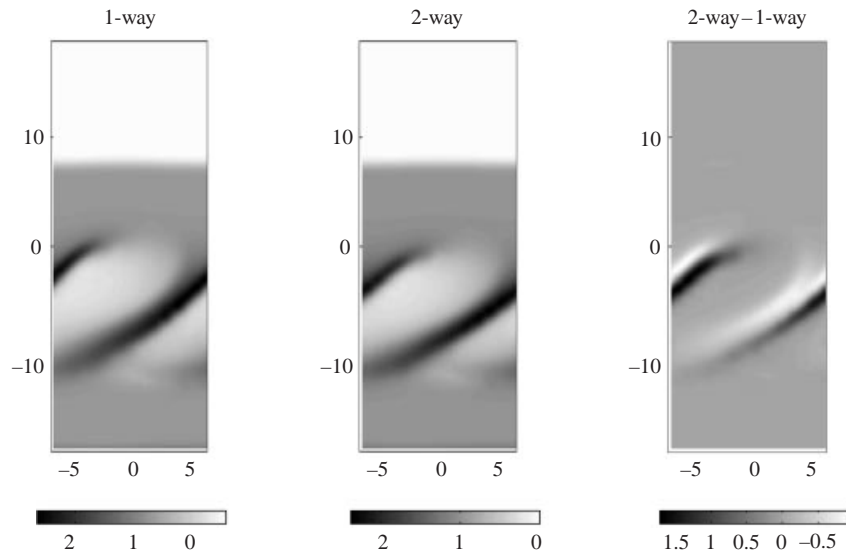
FIGURE 27. Particle concentration field for the flow shown in figure 25. The coupling effects are seen to result in a more rapid settling of the particles.
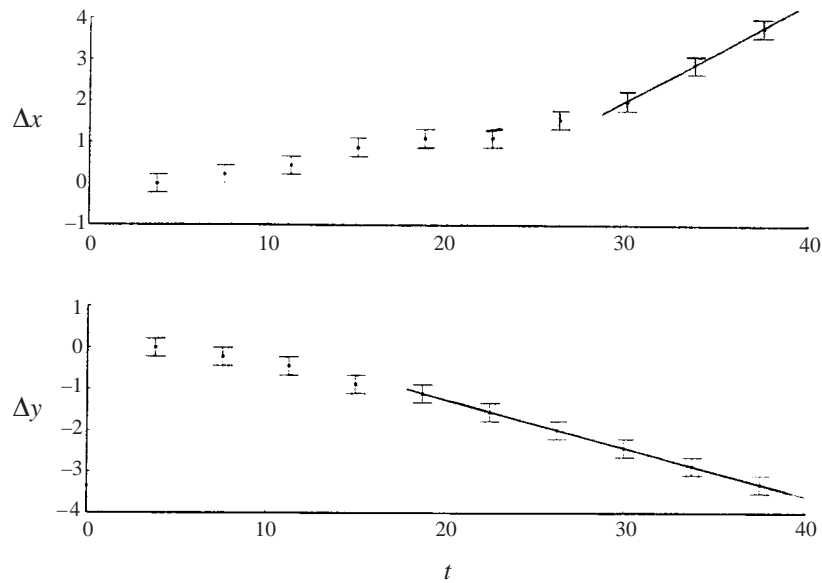

FIGURE 28. Displacement of the large-scale vortical structure in the horizontal and vertical directions, as evaluated from correlation data for $St = 3$, $Fr = 3$, $D = 0.5$. The error bars result from the resolution of the numerical grid. The straight lines represent least-squares fits of the data for $t > 18$.

numerical simulations furthermore reveal that for moderate settling velocities there exists an optimal coupling between the fluid and particle vorticity for intermediate values of the mass loading parameter, in the sense that the fluid vorticity maximum decays at the fastest rate. Interesting coupled dynamics are also observed for large settling velocities and intermediate mass loadings. Here, the transient evolution can
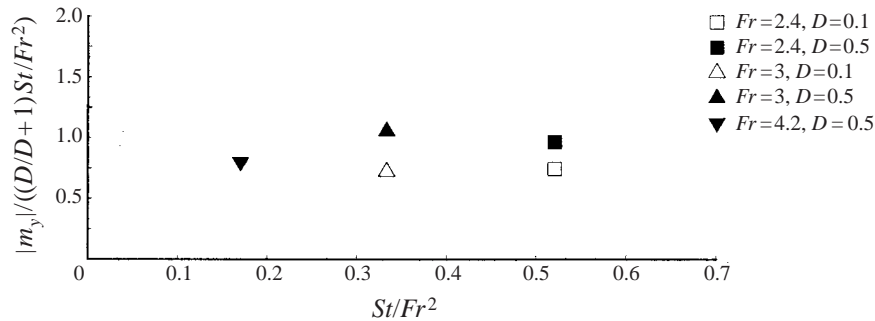
FIGURE 29. Comparison of the two-dimensional simulation results for the downward propagation velocity of the fluid vorticity field for $St = 3$ with the scaling law derived in §3. Here m_y indicates the rate at which the vertical position of the vortical structure changes with time. For the limited parameter range investigated here, reasonably good agreement is obtained.

produce vorticity profiles that exhibit more than one local maximum, resulting in multiple inflection points of the fluid velocity profile, which may have repercussions for the stability properties of the base flow. Based on the observation of a travelling-wave-type solution, downward flux arguments for the streamwise momentum can be employed to derive a scaling law for the propagation rates of the vorticity maxima.

For two- or three-dimensional particle-laden flow fields, the particle velocity in general will not be a single-valued function of space. However, frequently this assumption is made when establishing continuum-based Eulerian formulations of multiphase flow problems, in order to obtain less expensive computational problems. Within the present investigation, we have developed a mixed Lagrangian–Eulerian approach for two-way-coupled two-phase flows which is not subject to this limitation. It is similar in spirit to methods developed by Eaton, Elghobashi, Maxey and their respective coworkers; however, it is based on the vorticity variable rather than velocity and pressure. For uniformly loaded mixing layers, nonlinear simulations based on this method confirm some of the features observed by Druzhinin (1995b) for the model problem of a two-way-coupled particle-laden Stuart vortex, as well as by Dimas & Kiger (1998) in their linear stability analysis. In particular, for moderate and large values of the Stokes number the transport of vorticity from the braids into the core is seen to be slowed by the two-way coupling effects. As a result, the particle ejection from the vortex cores is weakened somewhat as well. For moderately large values of St, we also observe the formation of two bands of high particle concentration in the braids, an effect that clearly indicates the multi-valued nature of the particle velocity field, cf. also the one-way coupled analysis by Martin & Meiburg (1994). Interesting effects are observed for differentially seeded mixing layers, in which initially only one of the streams carries particles. Here the particle concentration gradient across the mixing layer leads to strong vorticity production and loss from the start, which results in an effective net motion of the vortex in the flow direction of the seeded stream.

If there is an appreciable settling velocity of the particles, the vortex propagates downward as well. By evaluating correlations of the vorticity fields at different times, an effective settling velocity of the vortex could be determined, which for the present range of parameters agrees well with the scaling law derived on the basis of unidirectional flow.

The present investigation has addressed only two-dimensional two-way coupling mechanisms between the two phases, i.e. the effect of the suspended phase on the

convection and diffusion of the carrier-phase vorticity. For the evolution of fully three-dimensional two-phase flows, an important aspect will be the influence of the particulate phase on the vortex stretching mechanism. One-way-coupled simulations (Marcu *et al.* 1995, 1996; Marcu & Meiburg 1996*a, b*) have already demonstrated that entirely new particle dynamics appear in three dimensions. For example, heavy particles can be stably located inside stretched vortices. The implications of these findings for two-way coupled three-dimensional flows are currently under investigation.

REFERENCES

AGGARWAL, S. K. & XIAO, Y. 1994 Effect of external forcing on droplet dispersion in a developing shear layer. *J. Prop. Power* **10**, 395–401.

CHANDLER, F. O. 1998 Convective instability of fluid interfaces. PhD thesis, University of Southern California.

CHEIN, R. & CHUNG, J. N. 1988 Simulation of particle dispersion in a two-dimensional mixing layer. *AIChE J.* **34**, 946–954.

CHEN, Y.-C. & CHUNG, J. N. 1995 The linear stability of an oscillatory two-phase channel flow in the limit of small Stokes number. *Phys. Fluids* **7**, 1510.

CHUNG, J. N. & TROUTT, T. R. 1988 Simulations of particle dispersion in an axisymmetric jet. *J. Fluid Mech.* **186**, 199–222.

CROWE, C. T., GORE, R. & TROUTT, T. R. 1985 Particle dispersion by coherent structures in free shear flows. *Part. Sci. Tech.* **3**, 149.

CROWE, C., SOMMERFELD, M. & TSUJI, Y. 1998 *Multiphase Flows with Droplets and Particles.* CRC Press, Boca Raton.

CROWE, C. T., TROUTT, T. R. & CHUNG, J. N. 1996 Numerical models for two-phase turbulent flows. *Ann. Rev. Fluid Mech.* **28**, 11–43.

DIMAS, A. A. & KIGER, K. T. 1998 Linear instability of a particle-laden mixing layer with a dynamic dispersed phase. *Phys. Fluids* **10**, 2539–2557.

DREW, D. E. 1983 Mathematical modeling of two-phase flow. *Ann. Rev. Fluid Mech.* **15**, 261–291.

DRUZHININ, O. A. 1994 Concentration waves and flow modification in a particle laden circular vortex. *Phys. Fluids* **6**, 3276–3284.

DRUZHININ, O. A. 1995*a* Dynamics of concentration and vorticity modification in a cellular flow. *Phys. Fluids* **7**, 2132–2142.

DRUZHININ, O. A. 1995*b* On the two-way interaction in two-dimensional particle-laden flows: The accumulation of particles and flow modification. *J. Fluid Mech.* **297**, 49–76.

DRUZHININ, O. A. 1997 The dynamics of a concentration interface in a dilute suspension of solid heavy particles. *Phys. Fluids* **9**, 315–324.

ELGHOBASHI, S. & TRUESDELL, G. C. 1992 Direct simulation of particle dispersion in a decaying isotropic turbulence. *J. Fluid Mech.* **242**, 655–700.

ELGHOBASHI, S. & TRUESDELL, G. C. 1993 On the two-way interaction between homogeneous turbulence and dispersed solid particles. I: Turbulence modification. *Phys. Fluids* A **5**, 1790–1801.

FINCHAM, A. M. & SPEDDING, G. R. 1997 Low cost, high resolution DPIV for measurement of turbulent fluid flow. *Exps. Fluids* **23**, 449–462.

FLECKHAUS, D., HISHIDA, K. & MAEDA, M. 1987 Effect of laden solid particles on the turbulent flow structure of a round free jet. *Exps. Fluids* **5**, 323–333.

GANAN-CALVO, A. M. & LASHERAS, J. C. 1991 The dynamics and mixing of small spherical particles in a plane free shear layer. *Phys. Fluids* A **3**, 1207–1217.

GOTTLIEB, D. & ORSZAG, S. A. 1977 *Numerical Analysis of Spectral Methods: Theory and Applications.* SIAM, Philadelphia.

HÄRTEL, C., NECKER, F., KLEISER, L. & MEIBURG, E. 1999 Direct numerical simulation of particle-driven gravity currents. In *Proc. First Symposium on Turbulence and Shear Flow Phenomena* (to appear).

HYLAND, K. E., MCKEE, S. & REEKS, M. W. 1999 Exact analytic solutions to turbulent particle flow equations. *Phys. Fluids* **11**, 1249–1261.

KATOSHEVSKI, D. & TAMBOUR, Y. 1993 A theoretical study of polydisperse liquid sprays. *Phys. Fluids* A **5**, 3085–3098.

KIGER, K. T. & LASHERAS, J. C. 1995 The effect of vortex pairing on the particle dispersion and kinetic energy transfer in a two-phase turbulent shear layer. *J. Fluid Mech.* **302**, 149–178.

KIGER, K. T. & LASHERAS, J. C. 1997 Dissipation due to particle/turbulence interaction in a two-phase, turbulent, shear layer. *Phys. Fluids* **9**, 3005–3023.

KIM, I., ELGHOBASHI, S. & SIRIGNANO, W. A. 1998 On the equation for spherical particle motion: Effect of Reynolds and acceleration numbers. *J. Fluid Mech.* **367**, 221–253.

KOUMOUTSAKOS, P. & LEONARD, A. 1995 High resolution simulations of the flow around an impulsively started cylinder using vortex methods. *J. Fluid Mech.* **296**, 1–38.

KULICK, J. D., FESSLER, J. R. & EATON, J. K. 1994 Particle response and turbulence modification in fully developed channel flow. *J. Fluid Mech.* **277**, 109–134.

LAWRENCE, G. A., BROWAND, F. K. & REDEKOPP, L. G. 1991 The stability of a sheared density interface. *Phys. Fluids* A **3**, 2360–2370.

LAZARO, B. J. & LASHERAS, J. C. 1989 Particle dispersion in a turbulent, plane, free shear layer. *Phys. Fluids* A **1**, 1035–1044.

LAZARO, B. J. & LASHERAS, J. C. 1992a Particle dispersion in the developing free shear layer. Part 1. Unforced flow. *J. Fluid Mech.* **235**, 143–178.

LAZARO, B. J. & LASHERAS, J. C. 1992b Particle dispersion in the developing free shear layer. Part 2. Forced flow. *J. Fluid Mech.* **235**, 179–221.

LELE, S. K. 1992 Compact finite difference schemes with spectral-like resolution. *J. Comput. Phys.* **103**, 16–42.

LEONARD, A. 1980 Vortex methods for flow simulation. *J. Comput. Phys.* **37**, 289–335.

LING, W., CHUNG, J. N., TROUTT, T. R. & CROWE, C. T. 1998 Direct numerical simulation of a three-dimensional temporal mixing layer with particle dispersion. *J. Fluid Mech.* **358**, 61–85.

LIU, J. T. C. 1966 Flow induced by an oscillating infinite flat plate in a dusty gas. *Phys. Fluids* **9**, 1716–1720.

MARCU, B. & MEIBURG, E. 1996a Three-dimensional features of particle dispersion in a nominally plane mixing layer. *Phys. Fluids* **8**, 2266–2268.

MARCU, B. & MEIBURG, E. 1996b The effect of streamwise braid vortices on the particle dispersion in a plane mixing layer. I. Equilibrium points and their stability. *Phys. Fluids* **8**, 715–733.

MARCU, B., MEIBURG, E. & NEWTON, P. 1995 Dynamics of heavy particles in a Burgers vortex. *Phys. Fluids* **7**, 400–410.

MARCU, B., MEIBURG, E. & RAJU, N. 1996 The effect of streamwise braid vortices on the particle dispersion in a plane mixing layer. II. Nonlinear particle dynamics. *Phys. Fluids* **8**, 734–753.

MARTIN, J. E. & MEIBURG, E. 1994 The accumulation and dispersion of heavy particles in forced two-dimensional mixing layers. I. The fundamental and subharmonic case. *Phys. Fluids* **6**, 1116–1132.

MAXEY, M. R. 1987 The motion of small spherical particles in a cellular flow field. *Phys. Fluids* **30**, 1915–1928.

MAXEY, M. R. 1990 On the advection of spherical and non-spherical particles in a non-uniform flow. *Phil. Trans. R. Soc. Lond.* A **333**, 289.

MAXEY, M. R., PATEL, B. K., CHANG, E. J. & WANG, L.-P. 1997 Simulations of dispersed turbulent multiphase flow. *Fluid Dyn. Res.* **20**, 143–156.

MAXEY, M. R. & RILEY, J. J. 1983 Equation of motion for a small rigid sphere in a nonuniform flow. *Phys. Fluids* **26**, 883–889.

MEIBURG, E. 1995 Three-dimensional vortex dynamics simulations. In *Fluid Vortices* (ed. S. Green). Kluwer.

MICHALKE, A. 1964 On the inviscid instability of the hyperbolic-tangent velocity profile. *J. Fluid Mech.* **19**, 543–555.

ORY, E., JOIA, I. A. & PERKINS, R. J. 1998 On the two-way interaction between a turbulent mixing layer and dispersed solid particles. *Eur. Turb. Conf.* pp. 277–280.

PAN, Y. & BANERJEE, S. 1996 Numerical simulation of particle interactions with wall turbulence. *Phys. Fluids* **8**, 2733–2755.

PARK, T. W., AGGARWAL, S. K. & KATTA, V. R. 1996 A numerical study of droplet-vortex interactions in an evaporating spray. *Intl J. Heat Mass Transfer* **39**, 2205–2219.

RAJU, N. & MEIBURG, E. 1995 The accumulation and dispersion of heavy particles in forced two-dimensional mixing layers. Part 2: The effect of gravity. *Phys. Fluids* **7**, 1241–1264.

RAJU, N. & MEIBURG, E. 1997 Dynamics of small, spherical particles in vortical and stagnation point flow fields. *Phys. Fluids* **9**, 299–314.

REEKS, M. W. 1991 On a kinetic equation for the transport of particles in a turbulent flow. *Phys. Fluids* A **3**, 446–456.

REEKS, M. W. 1992 On the continuum equations for dispersed particles in nonuniform flows. *Phys. Fluids* A **4**, 1290–1303.

RUETSCH, G. R. & MEIBURG, E. 1994 Two-way coupling in shear layers with dilute bubble concentrations. *Phys. Fluids* A **6**, 2656–2670.

SAFFMAN, P. G. 1961 On the stability of laminar flow of a dusty gas. *J. Fluid Mech.* **22**, 120–128.

SINCLAIR, J. L. 1997 Hydrodynamic modeling. In *Circulating Fluidized Beds* (ed. J. R. Grace, A. A. Avidan, T. M. Knowlton). Blackie Academic & Professional, London.

SIRIGNANO, W. A. 1993 Fluid dynamics of sprays – 1992 Freeman Scholar Lecture. *Trans. ASME: J. Fluids Engng* **115**, 345–378.

SOTERIOU, M. C. & YANG, X. 1999 Particle dispersion in variable density and viscosity shear flows. *Phys. Fluids* **11**, 1373–1386.

SQUIRES, K. D. & EATON, J. K. 1990 Particle response and turbulence modification in isotropic turbulence. *Phys. Fluids* A **2**, 1191–1203.

SUNDARAM, S. & COLLINS, L. 1999 A numerical study of the modulation of isotropic turbulence by suspended particles. *J. Fluid Mech.* **379**, 105–143.

TIO, K.-K., GANAN-CALVO, A. M. & LASHERAS, J. C. 1993a The dynamics of small heavy rigid spherical particles in a periodic Stuart vortex flow. *Phys. Fluids* A **5**, 1679–1693.

TIO, K.-K., LINAN, A., LASHERAS, J. C. & GANAN-CALVO, A. M. 1993b On the dynamics of buoyant and heavy particles in a periodic Stuart vortex flow. *J. Fluid Mech.* **254**, 671–699.

TRUESDELL, G. C. & ELGHOBASHI, S. 1994 On the two-way interaction between homogeneous turbulence and dispersed solid particles. II: Particle dispersion. *Phys. Fluids* **6**, 1405–1407.

UTHUPPAN, J., AGGARWAL, S. K., GRINSTEIN, F. F. & KAILASANATH, K. 1994 Particle dispersion in a transitional axisymmetric jet: A numerical simulation. *AIAA J.* **32**, 2004–2014.

WALLNER, E. M. 1998 Vorticity dynamics in two-way coupled particle laden mixing layers. Diploma thesis, University of Southern California/Universität Stuttgart.

WALLNER, E. & MEIBURG, E. 1998 Numerical simulation of two-way coupled particle laden mixing layers. *Proc. Third Intl Workshop on Vortex Flows and Related Numerical Methods, Toulouse, France, Aug. 24–27, 1998.*

WANG, L.-P. & MAXEY, M. R. 1993 Settling velocity and concentration distribution of heavy particles in homogeneous isotropic turbulence. *J. Fluid Mech.* **256**, 27–68.

WEN, F. & EVANS, J. 1994 Linear instability of a two-layer flow with differential particle loading. *Phys. Fluids* **6**, 3893–3905.

WILLIAMS, F. A. 1985 *Combustion Theory*, 2nd Edn. Benjamin/Cummings.

WINANT, C. D. & BROWAND, F. K. 1974 Vortex pairing: The mechanism of turbulent mixing layer growth at moderate Reynolds number. *J. Fluid Mech.* **22**, 237–255.

WRAY, A. A. 1991 Minimal storage time-advancement schemes for spectral methods. Preprint.

YANG, Y., CHUNG, J. N., TROUTT, T. R. & CROWE, C. T. 1990 The influence of particles on the spatial stability of two-phase mixing layers. *Phys. Fluids* A **2**, 1839–1845.